Emerging Indoor Photovoltaic Technologies for Sustainable Internet of Things

Vincenzo Pecunia,* Luigi G. Occhipinti, and Robert L. Z. Hoye*

The Internet of Things (IoT) provides everyday objects and environments with "intelligence" and data connectivity to improve quality of life and the efficiency of a wide range of human activities. However, the ongoing exponential growth of the IoT device ecosystem—up to tens of billions of units to date—poses a challenge regarding how to power such devices. This Progress Report discusses how energy harvesting can address this challenge. It then discusses how indoor photovoltaics (IPV) constitutes an attractive energy harvesting solution, given its deployability, reliability, and power density. For IPV to provide an eco-friendly route to powering IoT devices, it is crucial that its underlying materials and fabrication processes are low-toxicity and not harmful to the environment over the product life cycle. A range of IPV technologies—both incumbent and emerging—developed to date is discussed, with an emphasis on their environmental sustainability. Finally, IPV based on emerging lead-free perovskite-inspired absorbers are examined, highlighting their status and prospects for low-cost, durable, and efficient energy harvesting that is not harmful to the end user and environment. By examining emerging avenues for eco-friendly IPV, timely insight is provided into promising directions toward IPV that can sustainably power the IoT revolution.

1. Introduction

Society is in the midst of the so-called "Fourth Industrial Revolution" (Industry 4.0), in which there is a fusion of the physical, digital and biological spheres that will reshape the way people live and interact with each other.[1] A key pillar is the Internet of Things (IoT), which is a rapidly growing network of interconnected smart devices with access to the cloud.[2–4] Such devices enable daily objects and environments to acquire data connectivity and "intelligence," enhancing the quality of our daily lives and the efficiency of our businesses.[5–8] A substantial portion of the billions of new IoT devices that will be installed in the coming years are expected to be located inside buildings.[9] Currently, autonomous IoT nodes are most commonly powered using batteries.[10] However, batteries have a comparatively short lifespan, which limits the size and power consumption of the IoT devices, as well as the applications they can be used in, which need to compatible with battery replacement and maintenance.[10] Solely powering autonomous IoT devices with batteries may not sustain the growing complexity and size of the IoT ecosystem as it proceeds to one trillion nodes.[11,12] It is therefore important to develop energy harvesters that can act as suitable alternatives or work in conjunction with batteries.

A particularly promising route to addressing these challenges is to use photovoltaics (PV) to harvest ambient light inside buildings to power indoor IoT devices. Indeed, indoor photovoltaics (IPV) are widely deployable because of the common availability of lighting inside buildings and their reliance on radiative energy transfer. IPV harvest the energy from indoor lighting without emitting any greenhouse gases, and the devices can be scaled from the sub-mm^2 to >100 cm^2 area to power a wide range of different types of IoT electronics. Furthermore, IPV provide comparatively high power density among the various energy harvesting technologies that can be adopted indoors. Simultaneous with the rapid developments in the IoT, the past few years have also witnessed rapid developments in the performance and stability of a wide range of emerging materials for IPV.[13–15] However, a critical consideration that has yet to be addressed for IPV, and largely also for other types of energy harvesters, is their environmental sustainability, which involves having minimal negative impacts on

Prof. V. Pecunia
Jiangsu Key Laboratory for Carbon-Based Functional
Materials & Devices
Institute of Functional Nano & Soft Materials (FUNSOM)
Joint International Research Laboratory of Carbon-Based Functional
Materials and Devices
Soochow University
199 Ren'ai Road, Suzhou, Jiangsu 215123, China
E-mail: vp293@suda.edu.cn

Dr. L. G. Occhipinti
Department of Engineering
University of Cambridge
9 J J Thomson Avenue, Cambridge CB3 0FA, UK

Dr. R. L. Z. Hoye
Department of Materials
Imperial College London
Exhibition Road, London SW7 2AZ, UK
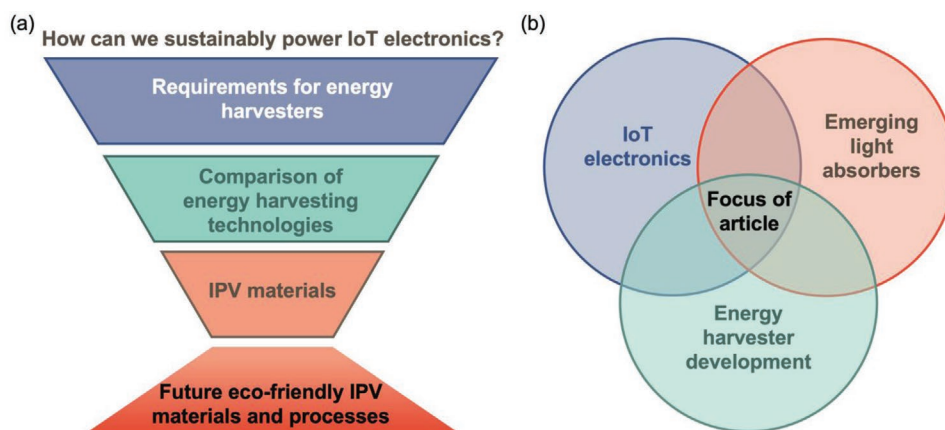E-mail: r.hoye@imperial.ac.uk

Figure 1. Scope of this Progress Report. a) Illustration of the flow of this article to address the question of how autonomous Internet of Things (IoT) devices could be sustainably powered, and b) the fields of research brought together in this article. This Progress Report discusses the environmental sustainability of IPV in terms of the toxicity of the materials used, the energy required for their fabrication, and the environmental impact of their manufacturing processes.

the environment—as can be determined through the life cycle assessment. Relevant impacts generally include climate change, ozone depletion, human toxicity and ecotoxicity, particulate matter, acidification, eutrophication, land use, and depletion of water and other resources (e.g., minerals and metals).[16] For instance, the materials used by the energy harvesters should not be hazardous to health or contain toxic elements that are regulated. Bringing together a discussion of the new materials developed for IPV with a focus on environmental sustainability will be important for guiding future materials selection efforts, as well as shaping future processing routes toward those with low toxicity and environmental impact.

This Progress Report begins by discussing the key requirements of energy harvesters for powering IoT nodes, before covering the energy sources available indoors and how they can be harvested. The potential of IPV is therefore put in context by comparing and contrasting them with alternative energy harvesters, to show the scenarios in which IPV are advantageous. The article then narrows down to focus on the established (hydrogenated amorphous silicon) and emerging materials (dye-based sensitizers, organics and lead-halide perovskites) for IPV, with emphasis on their performance, manufacturing and life cycle analysis. Finally, we discuss the new area of perovskite-inspired materials (PIMs) for IPV, and the requirements for designing efficient and environmentally friendly absorbers and manufacturing processes (**Figure 1**a). As such, this Progress Report brings together the fields of IoT electronics and energy harvesters with the field of emerging photovoltaic materials, especially perovskite-inspired absorbers.

From a terminological point of view, we will interchangeably use the phrases "environmentally sustainable" and "environmentally friendly" in the broad sense specified above (i.e., in relation to the set of environmental impacts provided earlier) as we introduce the IoT and various energy harvesting technologies in Sections 2 and 3, while we will resort to more specific wording when referring to particular sustainability aspects. Wherever relevant, we will also refer to the economic sustainability of the technologies discussed, intended as their ability to generate continuous economic growth. Further, in those cases

in which both environmental and economic sustainability are relevant to the discussion, we will simply refer to both as "sustainability" for the sake of conciseness. In regard to the subsequent discussion of various IPV technologies (Sections 4 and 5), owing to the sparsity of the associated literature on their sustainability assessment, our focus will be on the toxicity of the materials used, the energy required for their fabrication, and the environmental impact of their manufacturing processes. For the sake of brevity, we will nonetheless continue to use the phrase "environmentally friendly" in Sections 4 and 5, while tacitly referring to the selected sustainability aspects just specified.

2. The Need for Sustainable and Autonomous IoT Devices

2.1. Motivation and Market Potential of IoT Devices

Although heavily integrated into the consumer electronics market, the IoT extends far beyond handheld devices and home appliances. Indeed, the IoT is already supporting e-health (e.g., wearable, implantable, and swallowable smart devices), e-energy (e.g., smart meters, smart energy harvesting and storage), smart buildings (e.g., smart windows, smart heating, ventilation and air conditioning, and smart household appliances), smart cities (e.g., distributed air quality monitoring, smart cameras for traffic control and security, smart lighting, smart parking, and smart electric vehicle chargers), smart agriculture (e.g., vertical farming with smart lighting and distributed sensors for the monitoring of soil conditions and crops), connected cars, and Industry 4.0.[2,3]

Smart sensor systems[17] and wireless communications[18]—including digital technologies, low-power microprocessors and microcontrollers,[19,20] passive and active radio-frequency identification (RFID) tags,[21] wireless sensors, and ZigBee[22] and Bluetooth low-energy (BLE)[23] wireless communication technologies—are playing a key a role in the global development of the IoT, leading to the proliferation of sensor-rich portable devices. Such sensor-rich devices, combined with or used

**ADVANCED
SCIENCE NEWS**

www.advancedsciencenews.com

**ADVANCED
ENERGY
MATERIALS**

www.advenergymat.de

complementarily with an infrastructure-based computation substrate (e.g., the cloud), leverage mobility and processing power of the end-users to enhance their ability to sense, compute, and communicate even in the absence of reliable end-to-end connectivity. The combination of sensing, data processing, and data connectivity is essential for the IoT to equip daily objects and environments with "intelligence:" by sensing key physical quantities, processing the associated signals into information, and finally relaying such information to the end-users, the IoT enables more informed decisions to the benefit of our quality of life. It is important to appreciate that local data processing alone would not be sufficient to equip objects and environments with "intelligence." Indeed, much of this "intelligence" also rests on cloud computing and the interaction with the end-users, both of which require data connectivity.

The worldwide number of IoT devices is projected to increase to 43 billion by 2023, an almost threefold increase from 2018, as Internet connectivity becomes a standard feature for an increasing number of devices.[24] In fact, the rapid growth of the IoT ecosystem is expected to lead to one trillion interconnected devices by 2035.[25] The rapid growth of the IoT device ecosystem parallels its growth in market size. For instance, the global market for IoT end-user solutions reached US$ 100 billion in revenue for the first time in 2017 and forecasts suggest that this figure will grow to around US$ 1.6 trillion by 2025.[26] Meanwhile, the smart sensor market is predicted to reach a size of ≈US$ 90 billion by 2025.[27] Over the years, the number of low-power electronic devices powered by IPV cells has increased owing to the combined effects of cost reductions in both the electronics and IPV harvesters, as well as their respective performance improvements. By 2023 the IPV market for powering indoor wireless nodes is predicted to reach a value of US$ 850 million, with 60 million units sold per year, and is seen as the fastest growing sector of all nontraditional photovoltaic markets in the period 2019–2023.[10]

2.2. Need for Sustainability

Both the proliferation rate and the energy requirements of the IoT devices pose considerable challenges to the future growth and functional diversity of the IoT ecosystem. This is specifically so for IoT devices (hereafter referred to as IoT nodes) part of wireless sensor networks (WSNs), which are equipped with sensing capability and data connectivity and are being deployed ubiquitously to monitor key parameters of our daily objects and environments.[28] A key challenge associated with IoT nodes concerns their power supply.[29,30] A large number of IoT applications require such devices to operate autonomously without connections to the grid in order to ensure sufficient flexibility in their placement (e.g., indoors, outdoors, or mobile). The current mainstream approach to autonomous operation relies on the use of batteries—either primary (i.e., nonrechargeable) or secondary (i.e., rechargeable)—as the energy storage devices embedded in the IoT nodes to power their sensors, front-end electronics, data processing, and communication with a base station or with other IoT nodes.

The use of batteries to power the IoT nodes firstly poses considerable technical challenges, which critically impact the economic sustainability of the IoT. The most common batteries used to power autonomous IoT devices are primary batteries, such as alkaline and lithium batteries, as well as secondary batteries such as lithium-ion and lithium-polymer-based batteries.[30] Regardless of the type, all batteries inherently have a limited lifetime. Current IoT nodes based on ZigBee or BLE wireless communication protocols consume 10–100 µA on silent mode and 15–40 mA during data transmission and reception.[29] Even assuming a 1% duty cycle for a sensor node operating on a standard 3000 mAh battery, and neglecting the energy required by the front-end electronics, the microcontroller, and the sensors, the full discharge of the battery would occur after 8–25 months, which reduces to about 4–12 months when a minimum of 60% of the battery voltage is required for the IoT node to operate. This is compounded by the fact that IoT device applications typically pose tight constraints on the battery size, which should be in the centimeter-range or smaller. Despite considerable research efforts toward battery technologies with superior performance,[31–33] the limited energy density of primary batteries poses a critical challenge to their use as the sole power supply of the IoT sensor nodes. While the adoption of rechargeable batteries could potentially offer a solution, such batteries are also burdened by a limited number of charge-discharge cycles and a reduction in performance and energy storage density with each recharge cycle, in addition to the functional constraints resulting from the need to recharge them.

The technical limitations inherent in the reliance on batteries as the sole type of power supply of IoT nodes also result in considerable overhead maintenance costs of the IoT infrastructure and may not be economically sustainable. The need to frequently replace or recharge batteries is especially economically burdensome for IoT nodes placed in hard-to-reach locations, or for IoT nodes fully sealed or embedded in architectural elements and infrastructures, or in WSNs with a large number of IoT nodes. Indeed, it has been estimated that if batteries were relied upon as the sole power supply for autonomous IoT device operation, then it would not be possible to realize at least 80% of the potential of the IoT.[11] As the size of the IoT ecosystem grows, these issues will become more and more limiting. For instance, hundreds of millions of batteries would have to be replaced daily once the IoT ecosystem reaches the size of one trillion devices.[34]

In addition to the technical and economic considerations above, the exclusive reliance on batteries also brings along an important environmental sustainability challenge. For instance, if we consider lithium-based batteries, which constitute the dominant battery technology for IoT applications at present,[30,35,36] their production requires more than 50 times the energy that they can store, without taking into account the energy expenditure associated with materials sourcing and processing.[37] Additionally, lithium-based batteries rely on toxic and scarce materials such as lithium, cobalt, nickel, or manganese, whose extraction has considerable environmental impacts.[38–42] While more environmentally friendly battery technologies are currently being developed to address this environmental sustainability challenge, these new technologies are still not on par with mainstream battery technologies in terms of energy density,[41] hence their deployment in the IoT ecosystem would face similar technical as well as economic sustainability challenges.
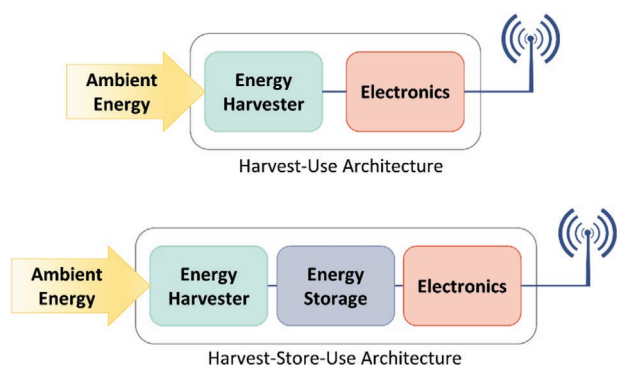
Figure 2. Schematics of energy harvesting architectures for IoT nodes. The power management unit is omitted for the sake of simplicity. The energy storage element could be a battery or a supercapacitor.

Figure 3. Key requirements for energy harvesters to be deployed to sustainably power the IoT.

In summary, the future growth of the IoT ecosystem critically depends on how to power its nodes that are to operate autonomously. The default strategy of exclusively relying on batteries is problematic in terms of technical viability, as well as economic and environmental sustainability. Therefore, to ensure that the IoT ecosystem can grow and deliver its full potential, it is key to identify alternative or complementary strategies that could overcome these sustainability challenges.

2.3. Energy Harvesting for a Sustainable IoT

To overcome the economic and environmental sustainability challenges associated with the exclusive reliance on batteries (Section 2.2), a promising approach is to power the IoT nodes by harvesting energy that is "freely" available in the surroundings of the nodes. This involves either ambient energy sources (e.g., light and radiofrequency (RF) waves) or human energy sources (e.g., body movements and temperature gradients near the body surface).[29,43] Energy harvesters (EHs) are then used to convert such energy into electricity.

Several energy harvesting configurations are possible. At a minimum, EHs could be deployed in combination with secondary batteries (which leads to the so-called harvest-store-use architecture with battery; **Figure 2**),[29,43–45] recharging them continuously and thereby delivering a solution with greater technical viability and economic appeal compared to battery-only alternatives. Further, EHs could also enable battery-based solutions with a higher environmental sustainability profile if used in combination with emerging green batteries, concurrently mitigating the impact of the lower energy densities of the latter.

Beyond battery-based approaches, EHs could potentially deliver the highest degree of economic and environmental sustainability in battery-less IoT node configurations. One possibility involves powering the IoT nodes directly with the energy supplied by EHs (which leads to the so-called harvest-use architecture; Figure 2).[43–45] Given that ambient energy may fluctuate over time, however, this approach is feasible only if the application allows intermittent operation and does not have strict latency requirements. By contrast, if the application requires the IoT node to have higher reliability and availability, the alternative, battery-less option
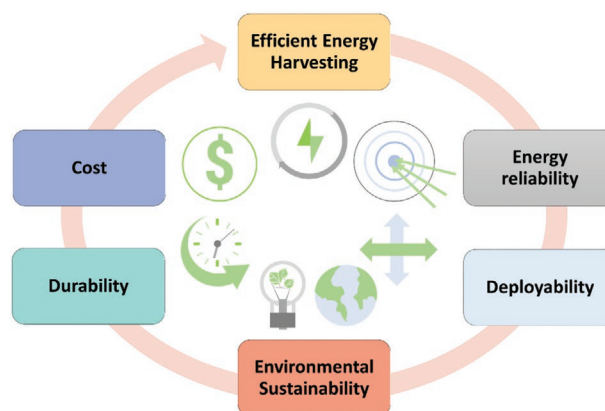
would be to store the energy supplied by the EH in a supercapacitor (harvest-store-use architecture with supercapacitor), which would thus act as an energy buffer.[29,44] Compared to the EH-battery combination, the use of the EH-supercapacitor architecture is particularly appealing, firstly because supercapacitor technologies are generally eco-friendlier.[46–49] Further, from a performance point of view, supercapacitors generally provide a much larger power density (i.e., power supplied per unit mass), by several orders of magnitude compared to batteries.[50] Additionally, while batteries provide a much higher energy density (i.e., energy stored per unit mass), supercapacitors allow much shorter recharge times by several orders of magnitude and have virtually unlimited cycle life.[50] All things considered, supercapacitors are particularly well suited for rapid energy storage/release, as needed to support the short bursts of activity (e.g., $\ll 1$ s) typical of IoT nodes (Section 2.5).

2.4. Requirements for Energy Harvesters to Power IoT Devices

For ambient energy harvesters to be used for powering IoT devices, they need to meet a number of requirements, which we discuss in this section. These requirements are schematically depicted in **Figure 3**.

2.4.1. Efficiency

A core functional requirement that EHs must meet is to provide sufficient energy and power to operate the IoT node of interest. The particular energy and power requirements depend on the application, the electronics technology and wireless communication protocol employed,[51,52] and the energy harvesting configuration adopted. The typical power consumption of personal and household devices and mainstream wireless communication protocols ranges from μW to W (**Figure 4**).

An important constraint on the capability of an EH technology to serve a given IoT application concerns the limited size typical of IoT nodes, which have characteristic dimensions ranging from 1 mm to 10 cm.[45,53–55] The overall power output of an EH is therefore closely linked to the power density of the associated energy source. The energy output of an EH
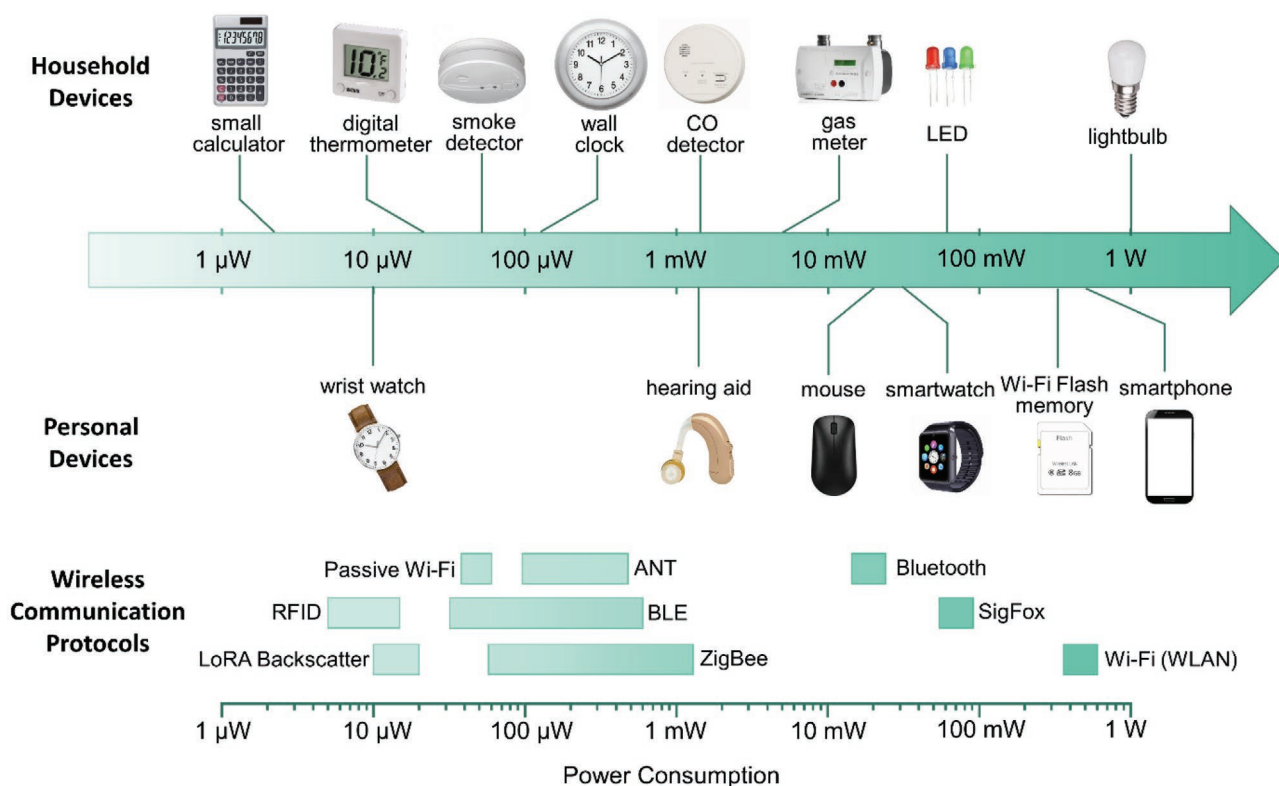
ADVANCED
SCIENCE NEWS
www.advancedsciencenews.com

ADVANCED
ENERGY
MATERIALS
www.advenergymat.de

Figure 4. Power consumption associated with typical household and personal devices and mainstream wireless communication protocols.[10,55,56]

additionally depends on its power conversion efficiency, which is defined as $PCE = P_{out}/P_{in}$, where P_{in} is the power from the energy source that reaches the EH and P_{out} is the corresponding power output of the EH. It follows that enhancing the PCE of a given EH technology would allow its use in more power-hungry devices or the reduction of the EH size and the overall footprint of the IoT node.

2.4.2. Energy Reliability

An EH is expected to supply energy with sufficient reliability so as to meet the power demands of the electronics in the associated IoT node. This aspect is particularly important because the energy source underlying a given energy harvesting technology may fluctuate over time (Section 3). While a harvest-store-use architecture can generally decouple the IoT node electronics from such fluctuations, relying on a predictable energy source would ensure a more reliable operation of the IoT node. Specifically, the predictability of an energy source concerns the possibility of forecasting the amount of energy that can be harvested and the time in which this energy is available.[29] A related aspect concerns the controllability of an energy source, which involves the possibility for the end-user of the IoT node to control the energy levels supplied and the time when the energy is available.[29,43] The energy level of a controllable energy source can be set and made available compatibly with the requirements of the application scenario at hand. Consequently, controllability does not refer to an energy source that supplies an exorbitantly high energy level to meet arbitrary energy demands, which

would be contrary to the purpose of ambient energy harvesting and the associated sustainability goals. Examples of predictable energy sources are RF radiation from TV and radio towers as well as indoor light, the latter also being controllable (**Table 1**). By contrast, ambient mechanical energy (e.g., as associated with ambient vibrations, pressure, and mechanical stress/strain) is typically not predictable, similar to the case of the energy available from the human body (Table 1).

A predictable energy source allows the corresponding EH to harvest energy reliably and potentially address a wider range of applications. Indeed, an IoT node equipped with an EH based on a predictable energy source can be designed for continuous operation and tighter performance requirements. Further, in combination with machine learning algorithms, predictions

Table 1. Predictability and controllability of representative energy sources.[29,43]

Energy source		Predictability	Controllability
Ambient RF	TV and Radio Towers	✓	✗
	Wi-Fi	✗	✗
Light	Solar	✓	✗
	Indoor light	✓	✓
Mechanical	Ambient indoor vibrations	✗	✗
	Pressure	✗	✓
	Stress–strain	✗	✓
Human	Finger motion, footfalls	✗	✓
	Physiological	✗	✗

ADVANCED
SCIENCE NEWS
www.advancedsciencenews.com

ADVANCED
ENERGY
MATERIALS
www.advenergymat.de

of the amount of energy available can be made more easily, enabling the optimized use of the harvested ambient energy beyond the periods during which it is available from its source.[57] On the other hand, an IoT node equipped with an EH that harvests energy from a controllable source can function reliably at the times when the energy is controllably supplied. Therefore, the energy reliability of an EH is closely linked to the nature of the energy source harvested.

2.4.3. Deployability

To find widespread use, an energy harvesting technology should ideally be application-agnostic. This concerns the deployability of the energy harvesting technology in terms of the range of locations where it can be used and the energy levels it can output to meet a diverse range of IoT applications. Consequently, an energy harvesting technology has greater deployability if it is based on an energy source that is predictable and widely accessible and a technology that is flexible in terms of form factor.

2.4.4. Environmental Sustainability

In view of their ultimate goal to sustainably power the IoT, it is of paramount importance to ensure that the corresponding EHs are environmentally sustainable. This concerns the environmental impacts (e.g., human toxicity, global warming, and eutrophication) associated with the sourcing of the base materials used in a given EH and its manufacturing process, use, and decommissioning at the end-of-life.[58] Important aspects that may ensure the environmental sustainability of a given EH technology concern the use of Earth-abundant and nontoxic base materials as well as low-energy manufacturing processes. It is especially important to use benign materials for the fabrication of EHs for the IoT because a wide range of IoT nodes are to be placed in daily objects and environments, hence in the vicinity of human end-users. Additionally, the particular importance of using abundant elements arises from the challenge inherent in the recycling of materials deployed in small, ubiquitous IoT nodes (e.g., as opposed to the recycling of EHs used in large-scale power plants), which would require the active participation of the end-users. Indeed, low collection rates have posed a significant challenge to recycling programs for consumer electronics to date.[39,59]

2.4.5. Durability

EHs are intended to enable IoT nodes to function well beyond the timescale of several months to ≈1 yr associated with battery recharging or replacement. In fact, the development of IoT nodes comprising EHs is motivated by the ultimate goal of perpetual device operation, for instance, as required for place-and-forget applications. Therefore, it is of paramount importance that EHs can deliver their nominal performance over a sufficiently long time. In consideration of application requirements, a realistic durability goal for IoT applications is that the EHs should have a device lifetime in the range of 10–20 yr.[60,61]

Importantly, depending on the EH technology considered, its indoor deployment may reduce the impact of or eliminate the stressors that would cause its performance degradation during outdoor operation (e.g., exposure to ultraviolet light, high humidity, and comparatively large temperature fluctuations), thereby leading to longer device lifetimes.

2.4.6. Cost

The realization of the full potential of the IoT would involve the use of one or multiple EHs per IoT node. In such a case, the number of EHs deployed would be on the same order of the size of the IoT device ecosystem. For this to be possible, the use of low-cost EH technologies is strongly beneficial. Apart from market dynamics, this points to the need to develop EH technologies that use Earth-abundant base materials, are simple, and are made with high-throughput fabrication methods.

2.5. Energy Management for Perpetual Operation

A common design goal for IoT nodes equipped with EHs concerns achieving perpetual operation. This firstly requires the adoption of a harvest-store-use architecture, so as to avoid downtimes of the IoT node due to the unavoidable fluctuations of the energy source being harvested. Further, it is critical to adopt low-power electronics and low-energy wireless communication protocols.[51,52,62,63] In fact, the greatest power dissipation in an IoT node occurs during wireless data transmission,[64] hence the communication protocol employed is a key determinant of the power that the EH is required to supply. In view of this, and assuming that a harvest-store-use architecture is used, the standard approach to minimize energy dissipation involves intermittent operation. In such a case, the IoT node spends long periods in a silent mode (during which the electronics has low power dissipation and an appreciable amount of energy can be harvested and stored) and switches to operation in an active mode (during which the sensors in the IoT node acquire the signals of interest and data is received/transmitted and processed) for much shorter periods (**Figure 5**).[65,66] Variations on the above are also possible, for instance, with data transmission occurring more sporadically
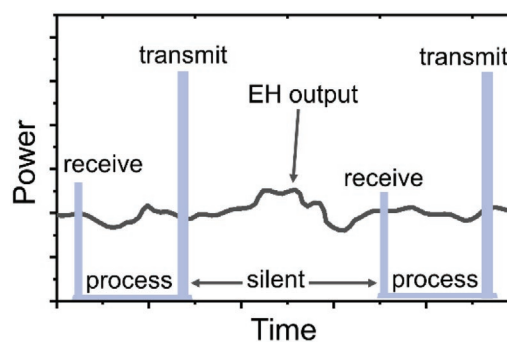

Figure 5. Schematic of power harvesting (black) and consumption (blue) in an IoT node based on a harvest-store-use architecture, which involves the node alternating between active and silent modes.
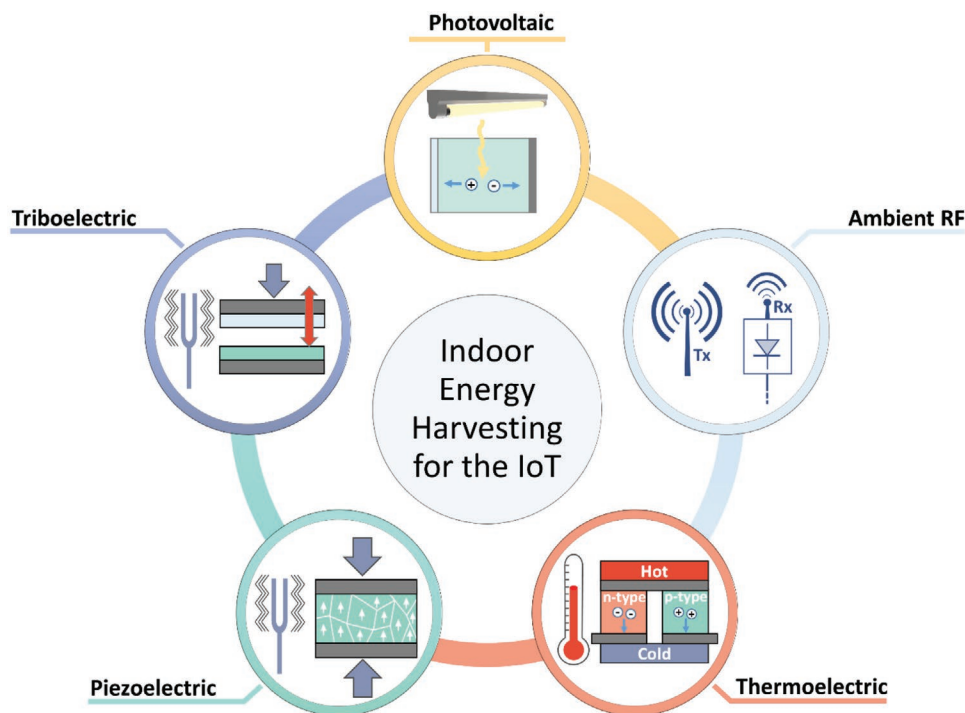
ADVANCED
SCIENCE NEWS
www.advancedsciencenews.com

ADVANCED
ENERGY
MATERIALS
www.advenergymat.de

Figure 6. Energy harvesting technologies for self-powered IoT devices, with schematics of the basic device architectures and energy conversion mechanisms.

than sensor signal acquisition and processing. Regardless, in a harvest-store-use architecture, the capability of an EH to allow perpetual operation closely depends on the duration of silent-mode intervals Δt_s that is tolerated by the corresponding application (Section 2.5) and the power dissipation $P_{diss,s}$ of the electronics in silent mode. If the power supplied by the EH is greater than $P_{diss,s}$ and if Δt_s is sufficiently long, then the surplus energy from the EH can be accumulated in the storage element during the silent-mode periods.[67,68] This would ultimately allow the IoT node to cope with the short bursts of high-power consumption during active-mode operation. Therefore, the power output of a given EH does not constitute the maximum IoT node power consumption that the EH is compatible with (e.g., in regard to the wireless communication protocols shown in Figure 2). It follows that adequate energy management is essential for EHs to deliver perpetual operation even in such cases in which the average power from the EH is considerably smaller than the instantaneous power during active mode operation.

3. Energy Harvesting for Autonomous IoT Devices

A large number of IoT applications involve indoor use (e.g., smart homes, smart manufacturing, e-health, and smart buildings). The realization of a sustainable IoT ecosystem therefore closely depends on the availability of suitable indoor energy harvesting solutions. In this section, we provide an overview of the main indoor energy harvesting approaches explored to date—i.e., thermoelectric, piezoelectric, triboelectric, ambient RF waves, and photovoltaic harvesting (**Figure 6**). Given the

ample literature on each of these approaches,[69–73] this section focuses on providing an overview of their properties in relation to the energy harvesting requirements discussed in Section 2, highlighting their strengths and weaknesses. This treatment will allow us to contextualize the important role that indoor photovoltaics could play in powering the IoT ecosystem.

3.1. Thermoelectric Energy Harvesting

Thermoelectric energy harvesters—also known as thermoelectric generators (TEGs)—convert waste heat into electricity. If a temperature difference ΔT is maintained between the end faces of a semiconductor slab, carriers will diffuse from the hot end to the cold end, thereby leading to the appearance of an electromotive force V_s (Seebeck voltage) proportional to ΔT (Seebeck effect): $V_s = \alpha \Delta T$, where α is the Seebeck coefficient.[74] In the context of indoor energy harvesting for the IoT, this effect can be used to harvest electricity from waste heat found in homes—e.g., waste heat from boilers, radiators, and appliances such as ovens—as well as in industrial settings—e.g., waste heat from furnaces and high-temperature machinery.[45,75] Regardless of the specific application scenario, a TEG needs to be in good thermal contact with the respective heat source and sink available, otherwise the thermal energy harvested is reduced (cf. PV and RF energy harvesting do not require direct contact to the respective energy sources). TEGs have also attracted considerable attention as a means of harnessing heat from the human body to power smart sensor nodes for health and wellness monitoring (e.g., as part of a wireless body sensor network).[76,77] Given the specificity of the aforementioned sources of waste
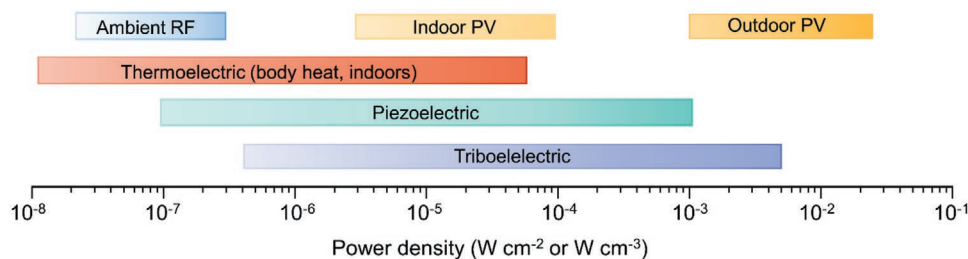
ADVANCED
SCIENCE NEWS
www.advancedsciencenews.com

ADVANCED
ENERGY
MATERIALS
www.advenergymat.de

Figure 7. Power densities supplied by various energy harvesting technologies (W cm^{-2} for PV, TEGs, TENGs, and ARFEHs; W cm^{-3} for PEGs).[10,67,77,91–103]

heat, it is apparent that TEGs could only be used to power dedicated sensor nodes in the immediate vicinity of such sources—i.e., they would be unsuitable to power sensor nodes placed in generic indoor locations. In relevant applications domains, however, TEGs are appealing due to their ability to provide electrical power without the direct emission of greenhouse gases, and with noise-free operation and no moving parts.

The unit component of a TEG is a thermocouple consisting of a p-type semiconductor and an n-type semiconductor placed electrically in series and thermally in parallel (Figure 6). Given that the values of the Seebeck coefficient in typical thermoelectric materials are in the region of 200–300 µV K^{-1}, a TEG normally consists of a large number of thermocouples (connected electrically in series and thermally in parallel) as a means of delivering appreciable voltage and electric power. For instance, a module comprising thousands of thermocouples is needed to obtain a voltage of ≈1 V in the presence of typical ambient temperature differences of ≈10 K—as relevant to IoT nodes to be placed on the human body or in homes.[45,50,78] While the indoor deployment of TEGs would obviously benefit from larger temperature gradients, these are only present in highly specific situations (e.g., in-store chillers in the retail sector and furnaces in the industrial sector), which often do not match with the locations where IoT nodes are widely needed.

The ultimate power conversion efficiency (PCE$_{TEG}$) of a TEG can be expressed as

$$PCE_{TEG} = \frac{T_H - T_L}{T_H} \frac{\sqrt{1 + ZT} - 1}{\sqrt{1 + ZT} + T_L/T_H} \qquad (1)$$

where T_H and T_L are the temperatures at the hot and cold ends of the TEG, respectively. ZT is the (dimensionless) thermoelectric figure of merit, which is defined as ZT $= S^2 \sigma T/\kappa$, where S is the Seebeck coefficient of the thermoelectric materials employed, σ its electrical conductivity, κ its thermal conductivity, and T is the average absolute temperature, $T = (T_H + T_L)/2$. Given the interdependence of the parameters determining ZT and their temperature dependence, efficiencies are generally low for ambient temperature differences of ≈10 K.[79]

Within the range of thermoelectric materials that have been explored,[80] mainstream TEGs adopt on Bi$_2$Te$_3$-based inorganic materials, which provide a ZT of ≈1 and power densities of <60 µW cm^{-2} in wearable applications (**Figure 7** and **Table 2**).[81,82] The use of Bi$_2$Te$_3$-based inorganic materials faces important challenges from an environmental point of view.[83] Indeed, Bi$_2$Te$_3$-based inorganic materials are burdened by the toxicity impact of their constituent elements and the chemicals involved in their extraction, as is the case for tellurium.[83] Their environmental profile is also negatively affected by their reliance on scarce elements (e.g., the scarcity of tellurium is comparable to that of platinum).[84] Further, the fabrication of conventional Bi$_2$Te$_3$-based TEGs may involve high-temperature and energy-intensive production methods,[85] such as long annealing steps at temperatures in the range of 400–850 °C and ingot dicing.[83,86] This leads to high electricity consumption and is associated with large emissions of greenhouse gases.[83]

The environmental impacts associated with mainstream thermoelectric materials have prompted researchers to investigate TEGs based on greener alternatives and fabrication methods. A particularly promising direction has been identified

Table 2. Key properties of indoor energy harvesting technologies.

EHs	Energy reliability	Deployability	Power density[a] [W cm^{-2} or W cm^{-3}]	Comments	Refs.
Thermoelectrics (TEGs)	Medium	Low–medium	10 n–60 µ	Applicable only in the immediate vicinity of a thermal source	[77,97–101]
Piezoelectrics (PEGs)	Medium	Low–medium	100 n–900 µ	Actuation required. Output highly dependent on actuation specs	[91,102,103]
Triboelectrics (TENGs)	Medium	Low–medium	400 n–50 m	Actuation required. Output highly dependent on actuation specs	[92,93]
Ambient RF (ARFEHs)	High	High	20–300 n	Ubiquitous in urban environments	[67,94–96]
Indoor PV (IPV)	High	High	3–100 µ	Predictable, controllable, and widely available	[10]

[a]Power density units are W cm^{-2} for IPV, TEGs, TENGs, and ARFEHs; W cm^{-3} for PEGs.

**ADVANCED
SCIENCE NEWS**
www.advancedsciencenews.com

**ADVANCED
ENERGY
MATERIALS**
www.advenergymat.de

in materials based on organic polymers as well as organic-inorganic hybrids.[82,87–89] While the ZT values of organic thermoelectric materials are in the range of 0.2–0.45 and thus lead to lower conversion efficiencies than Bi_2Te_3-based inorganic materials,[90] they rely on Earth-abundant elements and allow low-temperature processing such as printing.[87] The challenge of realizing high-performance n-type organic thermoelectric materials has led to the exploration of organic-inorganic hybrids with n-type character. In addition to their milder processing conditions, both the organic and organic-inorganic hybrid solutions enable TEGs that are mechanically flexible.[79] This leads to TEGs that could potentially cover a large fraction of the area of the waste heat source, thereby enhancing the power output of the TEG and positively contributing to their deployability.

3.2. Piezoelectric Energy Harvesting

Piezoelectric energy harvesters—also known as piezoelectric generators (PEGs)—convert mechanical stress into electricity. Such conversion requires the use of piezoelectric materials, which possess dipoles at the atomic or molecular scale (associated with asymmetric charge distributions or molecular groups) that vary in response to mechanical stress (Figure 6). The resulting charge density variations at the surfaces of a piezoelectric material lead to a voltage appearing across its opposite faces (piezoelectric effect), which can then be used to power electronic circuitry. Specifically, a PEG consists of a layer of a piezoelectric material placed between two electrodes in diverse geometric arrangements (e.g., a cantilever beam structure).[91] Under mechanical stress, the electric displacement field D in the material can be written in a simplified form as $D = d\,T + \varepsilon\,E$, where d is the direct piezoelectric charge coefficient, T is the mechanical stress, ε is the permittivity of the material and E is the electric field.[104] Importantly, the output power generated in a PEG is maximum if the stress is resonant with the natural frequency of the PEG.[91] Average power densities typically reported for PEGs are in the range of 100 nW cm^{-3}–900 µW cm^{-3} (Figure 7 and Table 2).[91,102,103]

The operation of a PEG requires a moving part (an actuator) that stresses the piezoelectric material. Therefore, in the context of indoor energy harvesting for the IoT, PEGs can be used as power sources only in the immediate vicinity of an actuator. For instance, actuation can be provided by body motion (e.g., as relevant to PEGs mounted on the human body to power smart sensors for health and wellness monitoring),[105] ambient vibrations (e.g., as induced by walking and the operation of home appliances or industrial machinery), and airflow (e.g., in combination with heating, ventilation, and air conditioning systems). Due to its association with motion, the application of PEGs is not only specific to the vicinity of an actuator but also suffers from the considerable variability (e.g., transient character) of its motion patterns. Additionally, if the PEG is not in good mechanical contact with the actuator, a fraction of the mechanical energy available may be lost, thereby reducing the overall conversion efficiency (by contrast, EHs relying on radiative transfer, such as PV and RF energy harvesters, do not require direct contact to the respective energy sources).

A dominant class of piezoelectric materials involves ceramics based on $Pb(Zr,Ti)O_3$ (lead zirconate titanate, PZT). The presence of lead—a toxic heavy metal—and the risk of releasing it into the environment during the life cycle of PZT-based PEGs (e.g., during calcination and sintering at temperatures >800 °C, as well as during machining) have prompted researchers to explore safer lead-free piezoelectric ceramics (Figure 10a).[106] This is consistent with the regulatory efforts in the direction of restricting the use of lead in electronics (e.g., Waste Electrical and Electronic Equipment (WEEE) and Restriction of Hazardous Substances directive (RoHS)).[107–109] In the search for lead-free alternatives, the most promising piezoelectric ceramics have been identified in materials based on $(K,Na)NbO_3$ (potassium sodium niobate, KNN).[110] However, the life cycle assessment of KNN-based materials has revealed that, while being lead-free, such materials have a greater environmental burden than PZT-based piezoceramics.[111] This is because KNN-based piezoceramics rely on niobium pentaoxide, which has negative environmental impacts (e.g., in terms of climate change and eco-toxicity), particularly in relation to raw material extraction.[111] Nonetheless, the use of KNN is to be preferred in consideration of the severe health hazards posed by lead-containing PZT-baser piezoceramics, especially in devices that are mounted on the human body or used in vivo.[111,112]

An alternative direction in the search for environmentally friendly piezoelectric materials involves the investigation of polymers, most importantly polyvinylidene fluoride (PVDF).[113–115] While less performant in terms of piezoelectric activity, piezoelectric polymers are attractive due to their flexibility (cf. the brittleness of piezoceramics), facile processing (e.g., via solution casting and electrospinning),[114] and biocompatibility.[116] Additional promising alternatives in terms of eco-friendliness have been identified in bio-derived or bio-inspired materials such as poly(ʟ-lactic acid) (PLLA) and cellulose.[114]

3.3. Triboelectric Energy Harvesting

Triboelectric energy harvesting for IoT applications involves the use of triboelectric nanogenerators (TENGs), which convert ambient mechanical energy into electricity through the combination of triboelectrification and electrostatic induction. When an external force brings two materials with different surface charge affinities in contact with each other, the surfaces of the two materials will become electrically charged (triboelectrification), especially in the presence of friction.[117] If the two materials are then separated, charges will flow through an external load connected to the two materials due to the potential difference existing between them (electrostatic induction).[118] The cycling of such a system between contact and separation will allow an alternating current to flow through the external load. While different device architectures can be used to realize such effects, the phenomena just described generally apply to all TENGs.[119] In addition to the materials involved and the device geometry and area, the electrical power output of a TENG also crucially depends on the force applied. Average power densities typically reported for TENGs are in the range of 400 nW cm^{-2}–50 mW cm^{-2} (Figure 7 and Table 2).[92,93] Similar to the case of piezoelectric energy harvesters, TENGs require

the presence of an actuator for them to supply electrical power and direct mechanical contact to it to fully exploit the available energy (in contrast to PV and RF energy harvesting, which do not require direct contact to the respective energy sources). Therefore, their applicability to power indoor IoT devices is specific to those cases in which actuation is available (e.g., human motion or acoustic vibrations)[93] and its randomness is compatible with the power constraints of the IoT devices to be powered/charged. Specifically, in regard to their indoor deployment, TENGs represent a highly promising energy harvesting approach to power nodes of body sensor networks, as needed for health and wellness monitoring.[120] Other specific applications involve the deployment of TENGs to power IoT nodes placed on household appliances and industrial machinery that generate mechanical vibrations.[121]

Typical materials used in the construction of TENGs include polymers placed between metal electrodes. Specifically, mainstream TENGs are made of poly(methyl methacrylate) (PMMA), fluorinated ethylene propylene (FEP), and polytetrafluoroethylene (PTFE).[119,122] Due to the inherent material simplicity of such devices and the adoption of flexible polymeric layers, TENGs can be constructed using simple, high-throughput, and low-energy-demand roll-to-roll manufacturing methods,[123] with the most complex fabrication steps involving the deposition and patterning of the electrodes. The environmental life cycle assessment of such TENGs has revealed that the energy consumption associated with their fabrication is dominated by the raw material requirements of the polymer layers.[124] Additionally, the use of acrylic polymers, as widely found in mainstream TENGs, constitutes the primary contributor to their environmental impacts, including carcinogenicity and CO_{2eq} emissions.[124] Nonetheless, in terms of eco-friendliness, the manufacturing of mainstream TENGs is considerably more benign than the fabrication of conventional photovoltaics, e.g., based on crystalline silicon, particularly due to the low-energy processes and relaxed material purity requirements associated with TENG fabrication.[124]

An active direction in TENG research involves the exploration of naturally occurring triboelectric materials directly found in plants (e.g., leaves) or obtained through plants processing (e.g., cellulose). This is expected to further improve the environmental profile of TENGs and to ensure their biocompatibility for implantable or wearable IoT applications.[125]

3.4. Ambient Radiofrequency Energy Harvesting

Ambient RF energy harvesting involves the conversion of ambient RF waves into electricity.[55] While RF waves are generally intended as any of the electromagnetic waves with frequencies in the range from ≈3 kHz to ≈300 GHz,[120] the frequencies relevant to ambient RF energy harvesting typically involve those associated with TV and radio transmission, cellular networks, and Wi-Fi routers. The RF waves emitted from such sources constitute ambient RF energy, as the respective sources are inherently intended for telecommunications and the energy made available through them would be present regardless of any energy harvesting purposes. In other words, ambient RF energy is practically "free" to use. This is in contrast to dedicated RF sources, which emit RF energy deliberately intended for power transfer. Dedicated RF power sources still benefit the development of the IoT in terms of relieving/reducing the need for batteries. However, energy harvesting from dedicated RF sources does not represent as attractive a solution as ambient RF energy harvesting from the point of view of power consumption, given that dedicated RF sources consume energy exclusively for power transmission. Consistent with the scope of this Progress Report, we thus focus on ambient RF energy harvesting in the rest of this section.

Ambient RF energy harvesting relies on radiative far-field wireless power transfer over a distance from several meters to several kilometers, depending on the specifics of the source and the particular ambient RF energy harvester (ARFEH) used.[71] Some of the ambient RF sources (e.g., TV and radio towers) are referred to as static because they provide continuous and comparatively stable power over time, thereby allowing the corresponding ARFEHs to be widely deployable. Other sources, such as Wi-Fi routers, are referred to as dynamic because their power output is intermittent, which severely limits the reliability of the associated energy harvesters. Further, RF sources vary greatly in terms of transmission powers: for example, while those associated with TV radio towers are in the range of 1 MW, they are reduced to less than 100 W for outdoor mobile network base stations, and to ≈0.1 W for Wi-Fi routers.[126] Further, the distance from the source is a key determinant of the amount of power that can be harvested. The ideal situation of free-space propagation would result in a reduction of the power density with d^{-2}, where d is the distance from the source.[127] However, scattering, absorption, and reflection effects due to unavoidable obstructions present in urban and indoor environments may lead to a more complex dependence on distance.[128] Regardless, surveys of indoor environments in urban locations have revealed that power densities commonly available for ambient RF energy harvesting are in the range of 20–300 nW cm^{-2} (Figure 7 and Table 2).[67,94–96] While the ongoing densification of Wi-Fi access points may increase the power density available, it has been shown that this would not be generally sufficient to power IoT nodes.[55] Therefore, despite ambient RF energy harvesting being attractive from the point of view of accessibility and, oftentimes, predictability, it currently suffers from particularly low power densities. Therefore, the deployment of ARFEHs based on existing technologies could be effective only in hybrid solutions combining them with other types of EHs, where ARFEHs would serve an additional energy supply.[129]

In terms of the components required for the construction of an ARFEH, the essential elements are a broadband antenna and a rectifying device.[71,130] Patch antennas are particularly appealing in terms of their environmental profile, as they lend themselves to low-temperature fabrication, e.g., through printing methods.[131] The possibility of fabricating antennas on biodegradable substrates such as paper has also been demonstrated.[132] Additionally, while rectifying circuits are commonly realized with conventional electronic components (typically, discrete Schottky diodes and CMOS diode-connected transistors),[133] which have considerable environmental impacts,[134] an attractive opportunity for environmentally friendly ARFEHs is offered by the recent developments of rectifying devices based on solution-processed semiconductors.[135,136]

3.5. Indoor Photovoltaics

IPV involves the conversion of ambient indoor light into electricity via the photovoltaic effect. Ambient indoor light is primarily from artificial sources, typically fluorescent (FL) and white light-emitting diode (WLED) lighting, which have emission spectra solely in the visible wavelength range (as opposed to the terrestrial solar spectrum relevant to outdoor PV, which has ≈50% of its power in the near-infrared wavelength range).[70] The key component of an IPV device is a semiconducting layer, which absorbs indoor light and converts it into electron–hole pairs. Such charges then travel in opposite directions toward the two electrodes sandwiching the semiconductor, thereby delivering an external electric current and a voltage (photovoltaic effect). While the operation and structure of an IPV device are similar to those of outdoor solar PV (i.e., solar cells), a crucial difference lies in the power and spectral content of the light sources involved. In addition to the spectral differences between indoor and outdoor illumination, the power density of indoor light sources is ≈60–300 μW cm^{-2}, i.e., approximately three orders of magnitude lower than that of terrestrial outdoor solar light.[137] Such differences are particularly consequential in terms of the operation and optoelectronic requirements of IPV devices. On the one hand, the fact that typical indoor light sources emit only in the visible range (see above) implies that the optimum bandgap for IPV is in the range of 1.9–2.0 eV[138,139] (by contrast, the optimum bandgap for outdoor solar PV is 1.1–1.4 eV due to the near-infrared component of the terrestrial outdoor solar spectrum).[140] On the other hand, the considerably lower intensity of indoor light sources inherently results in a reduction in the quasi-Fermi level splitting, and hence the open-circuit voltage (V_{oc}), compared to the case of terrestrial outdoor solar illumination. Assuming that the photocurrent varies linearly with the photogeneration rate (which is typically the case for an absorber with photovoltaic potential), then the efficiency would decrease as light intensity is reduced by an amount equal to $(nk_{B}T/q)\ln X$, as can be straightforwardly determined from the standard current–voltage model of a single-junction photovoltaic device.[141] Here, n is the ideality factor, k_{B} is the Boltzmann constant, T is the absolute temperature, q is the elementary charge, and X is the ratio between the reference light intensity (e.g., the light intensity equivalent to the photogeneration rate at 1 sun) and the light intensity of interest. Consequently, under the aforementioned conditions, the ideality factor is a key determinant of the efficiency at the reduced light intensities available in IPV operation. This implies that IPV efficiency would benefit from absorbers that do not feature deep levels (i.e., either defect tolerant or with successful defect healing strategies available)[142] and with no high majority carrier concentration near the contacts (e.g., from a space charge region).[143,144] Apart from the ideality factor, it is also important to consider the series and shunt resistances, which critically impact the overall shape of the current–voltage curve. In particular, while the effect of a finite series resistance is reduced as the light intensity is decreased, low shunt resistance values can be particularly detrimental in terms of fill-factor and overall efficiency at low optical power.[145] Therefore, it is particularly important to engineer IPV devices in order to prevent low-resistance paths within the absorber layer and the overall device stack.

In contrast to energy harvesting technologies that rely on spatially and time-constrained energy sources (e.g., a human actuator or a localized temperature difference), IPV is a widely deployable energy harvesting technology, given that it relies on near-ubiquitous indoor light and does not need to be placed in the immediate vicinity of the relevant energy sources. In other words, IPV is rather application-agnostic in terms of the type of IoT devices that it could charge/power. Further, IPV has high energy reliability, given the prolonged and largely predictable periods during which indoor light is available (refer back to Section 2.3 for a discussion of how EH can be coupled to energy storage for the perpetual operation of IoT devices). Hence, IPV shares a similar degree of reliability and deployability as ARFEH, insofar as both can be widely deployed within indoor environments to power the most diverse devices of the IoT ecosystem. Further, given the higher power density of indoor light compared to ambient RF radiation and the considerable efficiencies of current IPV technologies, IPV can deliver power densities (in the range of ≈3–100 μW cm^{-2}) that are orders of magnitude larger than those of ARFEH (Figure 7 and Table 2). Finally, several IPV technologies have been developed that have a promising environmental profile (Sections 4 and 5). In light of all this, IPV has obvious potential to play a preponderant role as an energy harvesting technology to sustainably power the IoT ecosystem. Therefore, we focus on IPV in the rest of this Progress Report.

4. Potential of Indoor Photovoltaic Technologies to Power IoT Devices

In outdoor light harvesting, crystalline silicon (c-Si) has become by far the dominant material in the PV industry, accounting for 94.5% of all solar cells produced worldwide in 2019.[146] This is due to the large scale of production, the technology being mature and well-established, the high stability, Earth-abundance, and low toxicity of silicon, as well as the bandgap (1.12 eV) being close to the optimum (1.34 eV) for absorbing AM 1.5G radiation. However, as discussed in Section 3.5, the optimum bandgap for IPV is in the range of 1.9–2.0 eV.[138,139] Hydrogen-passivated amorphous silicon (a-Si:H) has a bandgap of 1.6 eV, which is closer to this optimal range than c-Si, and has become one of the dominant IPV technologies.[10] The efficiency of a-Si:H IPV has reached up to 21%,[147] but most commercial a-Si:H IPV under WLED or FL lighting ranges from 4.4% to 9.2% (active device areas ranging from 1 to 38 cm^2),[147–149] well below the efficiency limit, which is close to 40% (**Table 3**).[138,148–152] Higher efficiencies have been achieved with III–V materials, reaching up to 21% for $Al_{0.2}Ga_{0.8}As$ under 508 lx WLED lighting.[10,139,153] While small-area III–V materials have potential for producing high power densities cost-effectively, their high fabrication costs limit the commercial competitiveness of large-area III–V modules for IPV.[153,154] Higher efficiencies have been achieved with three emerging classes of solution-processable materials: dye-sensitized solar cells (DSSCs), organic photovoltaics (OPVs) and lead-halide perovskites (LHPs). DSSCs and OPVs have demonstrated IPV efficiencies close to 30%.[14,155–157] LHPs have only emerged as a solar absorber over the past decade. However, like their progress for outdoor photovoltaics, LHP

Table 3. Comparison of the state-of-the-art performance, efficiency limit, and sustainability of established and emerging materials for indoor photovoltaics. Note that the energy payback time is calculated for 1 sun light harvesting. i-SLME values are detailed in **Table 4**. N.B.: n.r. means no report.

Material/property	IPV efficiency [%]	Active device area [cm²]	i-SLME [WLED; %]	i-SLME [FL; %]	Energy payback time [yr]	Toxicity and stability	Refs.
a-Si:H	21 (WLED), but most 4.4–9.2	1–38	41.4	38.6	1–3.5	• Si is benign • Pyrophoric SiH$_4$ precursor used, but this is managed at an industrial scale • Performance of a-Si:H decreases under illumination (light-induced degradation), which is related to the amorphous nature of the material and defects present; however light-induced degradation is less important under indoor illumination than 1 sun[158] • Device lifetime > 20 yr well established	[147–149,180,188,189]
DSSC (XY1/L1)	34.0 (1000 lx FL) 33.2 (1000 lx FL) 30.6 (1000 lx FL)	0.16$^{a)}$ 3.2 8	–	–	1–2	• Organic dyes make negligible contribution to overall toxicity profile of device, but Ru-based dyes increase toxicity profile • Solvents commonly used in processing have low toxicity • DSSCs with XY1/L1 sensitizer and Cu-based complex hole transport layer achieved no decrease in performance after 12 days of continuous operation in ambient air under periodic light/dark cycles. 1000 lx FL illumination was used[6] • DSSCs using hydrophobic dyes with extrapolated lifetimes of 25–40 yr demonstrated[202,203]	[6,15,188,198]
OPV (PM6:Y6-O)	31 (1650 lx WLED)	0.08	–	–	0.3–0.5	• No evidence of organic materials posing environmental threat • Some solvents used are toxic (e.g., chlorobenzene, chloroform) • Stability of polymer/nonfullerene blends to oxygen, moisture, heat, mechanical stress and irradiation needs to be established • Encapsulated OPV with polymer/nonfullerene blends have demonstrated: 1) no degradation in device performance after 1000 h testing under 1000 lx WLED illumination,[220] and 2) extrapolated device lifetime of 11 yr under 1 sun[218]	[14,189,214,218,220,223,225]
Lead-halide perovskite (MAPbI$_3$)	37.2 (1000 lx WLED)	0.10	48.2	44.5	<0.5	• Pb is a restricted element, is highly accessible, and bioaccumulates • Polar solvents that are currently widely used (e.g., DMF) are toxic • MAPbI$_3$ is unstable, but alternative compositions with improved thermal, photo- and environmental stability have been developed • Encapsulated IPV with MAPbI$_{2-x}$BrCl$_x$ have retained >95% of the original efficiency after 2000 h under 1000 lx FL light in ambient air[234] • Device lifetime >1 yr achieved under 1 sun through MAPbI$_3$ capped with 2D-perovskite protective layers[243]	[13,187,194,261,263,243]
BiOI	4.0 (1000 lx WLED) 4.4 (1000 lx FL)	0.0725	43.6	40.00	n.r.	• Non-toxic elements and precursors for scalable t-CVD growth • Thin films phase-stable after storage in ambient air for 197 days • IPV stable after storage for several months in glovebox with >1000 ppm O$_2$ and >500 ppm H$_2$O	[138,266]
Cs$_3$Sb$_2$I$_{9-x}$Cl$_x$	4.4 (1000 lx WLED) 4.9 (1000 lx FL)	0.0725	50.3	48.9	n.r.	• Low-toxicity elements • Precursors used for solution synthesis include hazardous DMF and toluene • IPV stable after storage for several months in glovebox with >1000 ppm O$_2$ and >500 ppm H$_2$O	[138]

Table 3. Continued.

Material/property	IPV efficiency [%]	Active device area [cm²]	i-SLME [WLED; %]	i-SLME [FL; %]	Energy payback time [yr]	Toxicity and stability	Refs.
FA$_{0.75}$MA$_{0.25}$SnI$_2$Br (doped with 1% Catechin)	12.81 (1000 lx)	0.0725	–	–	n.r.	• SnI$_2$ decomposition product lowers pH in aqueous media. However, the potential impact of HI in aqueous solution is under debate • Hazardous precursor solvents (e.g., DMF) used in thin-film growth • Devices retain >70% of initial efficiency after 400 min constant illumination in ambient air (72% relative humidity)	[267,268]
Ag$_3$BiI$_6$	n.r.[b]	–	56.2	48.7	n.r.	• Bi and I low-toxicity, but Ag$^+$ highly toxic. Toxicity of Ag mitigated if in compound form. • No evidence for Ag biomagnifying up food chain • Precursors used for solution synthesis include hazardous DMF • Ag$_3$BiI$_6$ PV retained >90% of initial 1 sun efficiency after storage for 45 days in ambient air (40% relative humidity)[269]	[270]
Cs$_2$TiBr$_6$	n.r.	–	45.1	40.7	n.r.	• Cs and Br low-toxicity • Toxicity of Ti depends on the form it is in, with Ti element being pyrophoric. TiBr$_4$ may evolve HBr, but likely in low quantities • Cs$_2$TiBr$_6$ powders decompose after 20 h[271] storage in ambient air • Cs$_2$TiBr$_6$ PV retain 94% of initial 1 sun efficiency when stored for 14 days at 70 °C, 30% relative humidity[272]	[193,271,272]

a)The unmasked device area is 0.25 cm²[6]; b)There is a recent report of IPV made from the related compound AgBiI$_4$, which has a power conversion efficiency of 5.17% under 1000 lx WLED lighting, giving a power output of 1.76 µW cm⁻². The active device area was 0.04 cm².[273]

IPV have demonstrated rapid progress, with 37.2% efficiency recently achieved under indoor lighting.[13] However, whether these emerging materials could become dominant in the IPV industry will depend on several factors beyond simply the performance under low illumination levels: 1) the scalability and costs of the manufacturing process, 2) stability and device lifetime, and 3) the environmental sustainability of the materials and manufacturing process over the entire life cycle of the IPV modules.[10] This section discusses these factors for established (a-Si:H) and emerging (DSSC, OPV, and LHP) types of devices for IPV, as illustrated in **Figure 8**. Another important topic is, of course, the role of interfaces and layers in the device stack on performance. However, this goes beyond the scope of this Progress Report, and we would refer readers to reviews written on this topic for a-Si:H PV,[158–161] DSSCs,[57,162–164] OPV,[165–168] and lead-halide perovskites.[169–172] We also note that in the discussion of life cycle analyses, we quote the energy payback time and kg-CO$_{2eq}$-kW$_p^{-1}$ values calculated for outdoor light harvesting because these analyses have not been so widely made for IPV applications, and because there is no standard indoor light spectrum or illuminance level, which makes it more difficult to compare the life cycle analyses conducted by different authors. However, the qualitative comparison between different technologies analyzed in the same way remains valid and relevant for IPV. We also note that the discussion on scalability in Section 4 focuses on the range of device areas and throughput currently achievable for different materials.

4.1. Hydrogenated Amorphous Silicon

In addition to its sub-optimal bandgap, the performance of c-Si for IPV is limited by its low shunt resistance. This leads to a substantial reduction in the V_{oc} and fill factor (FF) at low illumination levels.[139] a-Si:H overcomes this limitation by having a high shunt resistance, such that the dark current does not play a dominant role under low illuminance.[139,158] The wider bandgap of a-Si:H compared to c-Si, in addition to the higher ratio of photo- to dark-conductivity, leads to the devices producing a higher V_{oc} in excess of 0.5 V under indoor lighting, which has the advantage of being sufficient to operate many electronic circuits without requiring the IPV devices to be connected in series.[158] a-Si:H is an alloy, and 10 at% H would typically be incorporated into a-Si used in thin-film solar cells. The H plays the role of passivating dangling bonds that inevitably form as a result of the amorphous structure of silicon (Figure 8a).[158] Indeed, it is the defects present (both mid-gap levels, as well as band-tail states arising from the amorphous structure) in the material and those forming at interfaces that limit the efficiency of a-Si:H for PV and IPV applications,[158,175–178] such that the efficiencies are well below the radiative limit (**Figure 9**). These defects also limit the charge-carrier diffusion lengths, and an electric field is required across the entire active layer in order to assist carrier collection. As a result, a-Si:H devices adopt an intrinsic layer sandwiched between p- and n-doped a-Si:H layers (Figure 8e), such that the intrinsic active layer is depleted.[158] Defects may also play a role in limiting the stability of a-Si:H solar cells through light-induced processes. These include substantial irreversible
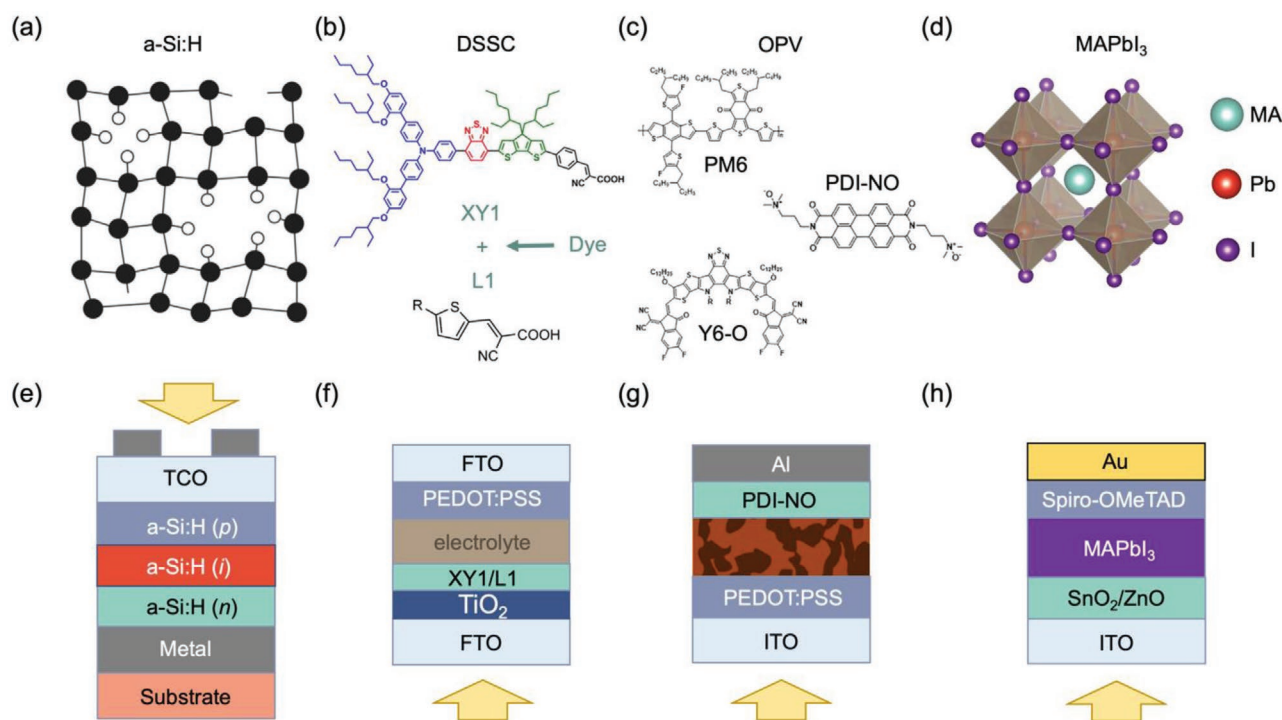
**ADVANCED
SCIENCE NEWS**
www.advancedsciencenews.com

**ADVANCED
ENERGY
MATERIALS**
www.advenergymat.de

Figure 8. a–d) Crystal/molecular and e–h) device structure of established and emerging materials for indoor photovoltaics: a,e) hydrogenated amorphous silicon, or a-Si:H, b,f) dye-sensitized solar cells, or DSSC, c,g) organic photovoltaics, or OPV, d,h) methylammonium lead iodide (MAPbI$_3$) perovskite. The crystal structure in (a) Reproduced with permission.[158] Copyright 2017, Elsevier. The molecular structure of XY1 in (b) Reproduced with permission.[173] Copyright 2016, American Chemical Society. The molecular structure of L1 in (b) Reproduced with permission.[174] Copyright 2007, American Chemical Society. The molecular structure of PM6, Y6-O and PDI-NO in (c) Reproduced with permission.[14] Copyright 2020, Cell Press.

reductions in device performance (light-induced degradation), as well as reversible processes, such as the Staebler–Wronski effect, which involves light-induced reductions in photoconductivity that can be reversed through annealing at above 150 °C.[158,179] Light-induced degradation is particularly harmful and can cause the a-Si:H device to lose 10–20% of the initial efficiency during the first few months of operation. However, the degradation rate afterward is similar to those of other commercial PV technologies, at ≈1% yr^{-1},[158,180] and a-Si:H devices are adequate for powering small electronics with a lifetime of at least 20 yr.

a-Si:H is a mature technology, and there is little difference between the efficiencies of laboratory-scale solar cells and industrially produced modules.[158,182] Typically, a-Si:H is grown at scale by plasma-enhanced chemical vapor deposition (PECVD), and can be used to manufacture modules with >1 m^2 area.[158,183] Currently, a-Si:H devices are sold at low production volumes (<10 m^2 yr^{-1}) for US$ 0.2 cm^{-2}.[10] However, market demand for IPV is expected to grow from 10^2 m^2 yr^{-1} (currently) to 10^5 m^2 yr^{-1} over the next 5 yr,[184] and it is expected that a-Si:H sold at large volumes to the wireless sensors market would be substantially lower cost than the current generally available price.[10]

The manufacturing of a-Si:H has a comparatively low ecological impact, owing to the low processing temperatures used (typically <300 °C) compared to c-Si.[185,186] For outdoor PV applications, the energy payback time (time required for energy produced from PVs compared to energy required for manufacturing the module)[187] of a-Si:H has been estimated to be only 1–3.5 yr.[180,188,189] Silicon itself is a benign and abundant element (**Figure 10**a), with an annual production of 7 × 10^6 tonne yr^{-1})[190] worldwide. Although the growth of a-Si:H by PECVD involves the use of silane, which is pyrophoric, this is managed in industrial processes by combusting waste gases.[180] However, life cycle analyses have identified that a factor limiting traditional a-Si:H manufacturing is the high wastage of the silane precursor, in which 85% of the precursor is not used and therefore combusted. This leads to an embodied energy of 1200 MJ eq. m^{-2} for a-Si:H modules. While this is lower than for c-Si (23 000 MJ eq. m^{-2} for single-crystalline silicon),[191] life cycle analyses have shown that reducing the wastage of silane through recycling can lower the overall embodied energy per module by 5.7 MJ eq. m^{-2}, which can lead to substantial savings in a gigawatt-level production facility.[180]

4.2. Dye-Sensitized Solar Cells

DSSCs involve the use of a light-absorbing dye mounted on a mesoporous scaffold (typically TiO$_2$) and interfaced with a redox mediator. The excitons generated in the dye following light absorption are separated at the interface with TiO$_2$, to which the electron is injected, while the hole is used to oxidize the adjacent redox couple,[195,196] which is then reduced again by the electron injected from the counter-electrode. Some of the dyes used have bandgaps close to the 1.9–2.0 eV optimum value

Table 4. Input (E_g) and calculated (f_r, J_{sc}, V_{oc}, and SLME) parameters for thin-film absorbers for Figure 13. The room temperature space group of the materials is also tabulated. Note: it was assumed that the absorbance below the optical bandgap is 0, and that the film thickness was 500 nm in all cases.

Material	Space group	E_g [eV]	f_r[a]	J_{sc} [μA cm^{-2}]		V_{oc} [V]		SLME [%]	
				FL	WLED	FL	WLED	FL	WLED
a-Si:H		1.61	1	117	113	1.30	1.30	38.6	41.4
MAPbI$_3$	$I4/mcm$	1.59	1	145	143	1.21	1.21	44.5	48.2
Ag$_3$BiI$_6$	$R\overline{3}m$	1.86	1	131	137	1.45	1.45	48.7	56.2
BiI$_3$	$R\overline{3}H$	1.82	0.003	142	145	1.17	1.17	41.6	47.0
InI	$Cmcm$	2.00	1	117	118	1.58	1.58	47.7	53.2
Sb$_2$S$_3$	$Pnma$	1.65	0.044	143	143	1.18	1.18	42.6	47.3
Cs$_2$SnI$_6$	$Fm\overline{3}m$	1.3	1	122	123	1.08	1.08	32.9	36.7
Cs$_2$TiBr$_6$	$Fm\overline{3}m$	1.7	0.001	144	145	1.13	1.13	40.7	45.1
Cs$_3$Sb$_2$I$_9$ (0D)	$P6_3/mmc$	1.95	0.001	133	123	1.35	1.35	45.7	46.8
Cs$_3$Sb$_2$(I,Cl)$_9$ (2D)	$P\overline{3}m1$	1.95	0.204	135	125	1.42	1.42	48.9	50.3
Rb$_3$Sb$_2$I$_9$	$P2_1/n$	2.10	0.004	105	91	1.54	1.54	41.4	39.6
(MA)$_3$Sb$_2$I$_9$	$P6_3/mmc$	2.14	0.044	81	80	1.63	1.63	34.2	37.3
(FA)$_3$Bi$_2$I$_9$	—[b]	2.19	1	75	65	1.77	1.77	34.7	33.2
BiOI	$P4/nmm$	1.93	0.459	104	103	1.50	1.50	40.0	43.6
Cs$_3$Bi$_2$I$_9$	$P6_3/mmc$	2.20	0.001	70	61	1.62	1.62	29.1	28.3
Cs$_2$AgBiBr$_6$	$Fm\overline{3}m$	2.25	0.001	75	76	0.71	0.71	12.6	14.0

[a]Fraction of recombination events that are radiative, calculated from $f_r = e^{-\left(\frac{E_g^{da} - E_g}{k_B T}\right)}$, where E_g^{da} is the first direct transition and E_g the optical bandgap, k_B Boltzmann's constant and T temperature. The floor in the value of f_r was set to 0.001 because it was believed that beyond this threshold, the difference between the direct transition and optical bandgap would not be a good indicator of the level of nonradiative recombination; [b]Computed crystal structure reported to be distorted hexagonal, such that it is technically monoclinic.[302]

for IPV,[10,155] and 34.0%-efficient DSSC IPVs under 1000 lx FL lighting has been achieved (0.16 cm^2 masked active device area).[6] This was realized using a combination of a benzothiadiazole-based donor–acceptor-π-acceptor dye (abbreviation: XY1)[173] along with an organic dye (abbreviation: L1),[174] and the molecular structures of the dyes can be found in Figure 8b. These dyes were sensitized on a mesoporous TiO$_2$ scaffold, and a Cu^{2+}/Cu$^+$ redox couple was used as the electrolyte. The co-sensitized DSSCs demonstrated higher photovoltages and efficiencies than devices using only one of the dyes alone, and this was attributed to improved coverage of the mesoporous TiO$_2$ scaffold by the sensitizers.[6]

Historically, DSSCs have used liquid electrolytes, and this commonly features in the current generation of commercialized DSSCs.[197,198] There are numerous companies commercializing DSSCs, which are expected to have a competitive advantage over crystalline silicon solar cells under indoor lighting, as well as for building-integrated PV.[198] In 2020, the market worth of DSSCs was US$ 100 million, and the expected compound annual growth rate is 12.4% until 2027.[199] However, the use of liquid electrolytes limits the long-term device stability (particularly the thermal stability) of the DSSC, owing to the degradation of the electrolyte itself, or changes at the electrolyte-TiO$_2$ interface, which can be accentuated by the incorporation of water and oxygen during device fabrication or operation.[200,201] Improved stabilities have been achieved using hydrophobic dyes that do not incorporate moisture during device fabrication, and these devices were tested for 2.5 yr at 0.8 sun at 55–60 °C, demonstrating only a 17% reduction in efficiency. From these accelerated degradation tests, the module lifetime was predicted to be 25–40 yr, although the efficiency of these DSSCs using hydrophobic dyes was only ≈4% under 1 sun.[202,203] In addition to alternative dyes, the research field has also looked into more stable alternatives to liquid electrolytes, such as ionic liquids, quasi-solid systems (e.g., gels) and solid-state hole transport layers.[197,198] Solid-state hole transport materials include organic small molecules (e.g., spiro-OMeTAD) and copper-based complexes.[6] These copper-based complexes were originally dissolved in organic solvents and used to form the Cu^{2+}/Cu$^+$ redox couple. However, it was recently found that drying the electrolyte to form a solid-state copper-based hole conducting layer led to DSSCs with comparable or improved efficiencies, along with stable performance under both indoor and 1 sun illumination.[6,57,204,205]

DSSC modules have been manufactured since 2009, and benefit from being compatible with existing large-area thin film deposition and roll-to-roll processing technologies.[203] These include screen printing, which is used to deposit the TiO$_2$ layer. As a result, DSSC modules with >100 cm^2 active area are manufactured by several companies.[206] In addition to rigid modules (commonly used for building-integrated PV), flexible modules are also manufactured, and a roll-to-roll processing capability of 800 m in 3 h has been reported.[206]
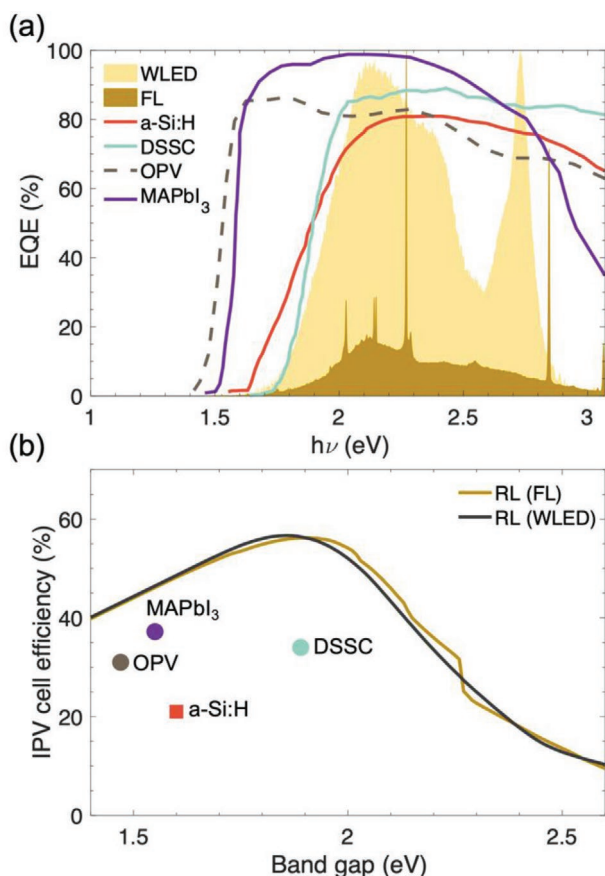
**ADVANCED
SCIENCE NEWS**

www.advancedsciencenews.com

**ADVANCED
ENERGY
MATERIALS**

www.advenergymat.de

Figure 9. Performance of established and emerging materials for indoor photovoltaics. a) Comparison of the external quantum efficiency (EQE) spectra of the devices against the while light-emitting diode (WLED) and fluorescent light (FL) spectra, both at 1000 lx. b) Power conversion efficiency of state-of-the-art devices compared to the radiative limit (RL). a-Si:H, OPV and MAPbI$_3$ devices measured under WLED lighting, while the DSSC was measured under a warm white 18 W fluorescent tube.[6,13,14,181] Device performance data (EQE and power conversion efficiency). a-Si:H,[147,181] DSSC,[6] OPV,[14] MAPbI$_3$ perovskite.[13] The spectra for the light sources.[138] Please note that in the case of the OPV and DSSC devices, the bandgap was determined from the inflection point of the EQE curve.

The highest temperature process required in the manufacture of DSSCs is the sintering of the TiO$_2$ layer, which takes place at 450–500 °C. The deposition of other layers takes place at lower temperatures, especially since many dyes degrade at temperatures above 100 °C.[203,207] As a result, a life cycle analysis of DSSC modules on glass or flexible polyethylene terephthalate substrates found that the energy payback time for outdoor light harvesting applications was only 1–2 yr, with kg CO$_{2eq}$ kW$_p^{-1}$ values approximately half of that of a-Si.[188]

In terms of environmental sustainability, historically, many of the dyes used in DSSCs were based on Ru, which is a scarce element that increases the overall toxicity profile of the device.[188] As a result, there have been efforts to replace Ru-based dyes with organic dyes, and these have indeed yielded the most efficient DSSC-based IPV, as discussed above.[15] However, it has been found that organic sensitizers do not improve the overall sustainability profile, owing to the use of harmful

reactants, solvents, and catalysts.[198] Natural dyes (e.g., sourced from plants) have also been considered, but the efficiency and stability of the resulting DSSCs are lower than devices based on synthetic dyes.[198] Beyond the sensitizer, the electrolyte also plays an important role in the overall sustainability profile of the devices. As discussed above, historically, DSSCs were based on liquid electrolytes containing volatile and flammable organic solvents, as well as corrosive redox couples. However, the quasi-solid electrolyte alternatives that have been developed do not have an improved sustainability profile over traditional liquid electrolytes because they are based on the same salts, solvents and additives.[198] The synthesis and disposal of ionic liquid alternatives are also not sustainable.[208] For solid-state alternatives, spiro-OMeTAD suffers from sensitivity to oxygen and moisture, as well as high synthesis costs.[198] On the other hand, an improved sustainability profile may be achieved using copper-based complexes as hole transport layers, and in-depth life cycle analyses should be performed.[198] A potential limiting factor may be the current practice of introducing these layers to the DSSC by dissolving the complexes in the same organic solvents originally used in liquid electrolytes,[6,204,205] and alternative routes for depositing this layer may need to be developed. Another route to improve the sustainability profile of DSSCs is through water-based DSSCs.[163] However, to fabricate the most efficient devices, ultrapure water is needed, and the energy-intensive purification process decreases the sustainability profile and increases the overall cost of the process.[198] Furthermore, beyond the sensitizer, redox couple and electrolyte, consideration needs to be given to the counter-electrode, as well as the processing of the transparent conducting oxide on glass substrates, and these are detailed in several reviews.[198,209,210] Thus, DSSCs are a promising technology for IPV that have demonstrated efficient performance under low illumination levels. However, further work is still needed to develop sustainable and stable components in these devices.

4.3. Organic Photovoltaics

Conjugated organic small molecules and polymers exhibit semiconducting behavior and have been widely explored for photovoltaics. Unlike c-Si, organic materials have low dielectric constants and high exciton binding energies. Therefore, photon absorption leads to the generation of excitons rather than free carriers. This is similar to DSSCs, and as with DSSCs, the exciton needs to be separated into electrons and holes that are injected into separate charge transport layers. In organic photovoltaics, this is often achieved through the use of bulk heterojunctions, which comprise an electron-donating organic compound (e.g., a conjugated polymer or small molecule) intimately mixed with an electron-accepting organic compound (e.g., a fullerene, such as PC$_{71}$BM).[211,212] Not only does this produce a spatially distributed heterojunction (i.e., a bulk heterojunction) to separate the excitons, but this also ensures that the distance excitons need to travel before reaching the donor–acceptor interface is within the exciton diffusion length, which is typically on the order of 10 nm in organic semiconductors.[156,213,214] Organic photovoltaics (with an active device area of 0.08 cm^2) have reached efficiencies of 31% under indoor

**ADVANCED
SCIENCE NEWS**

www.advancedsciencenews.com
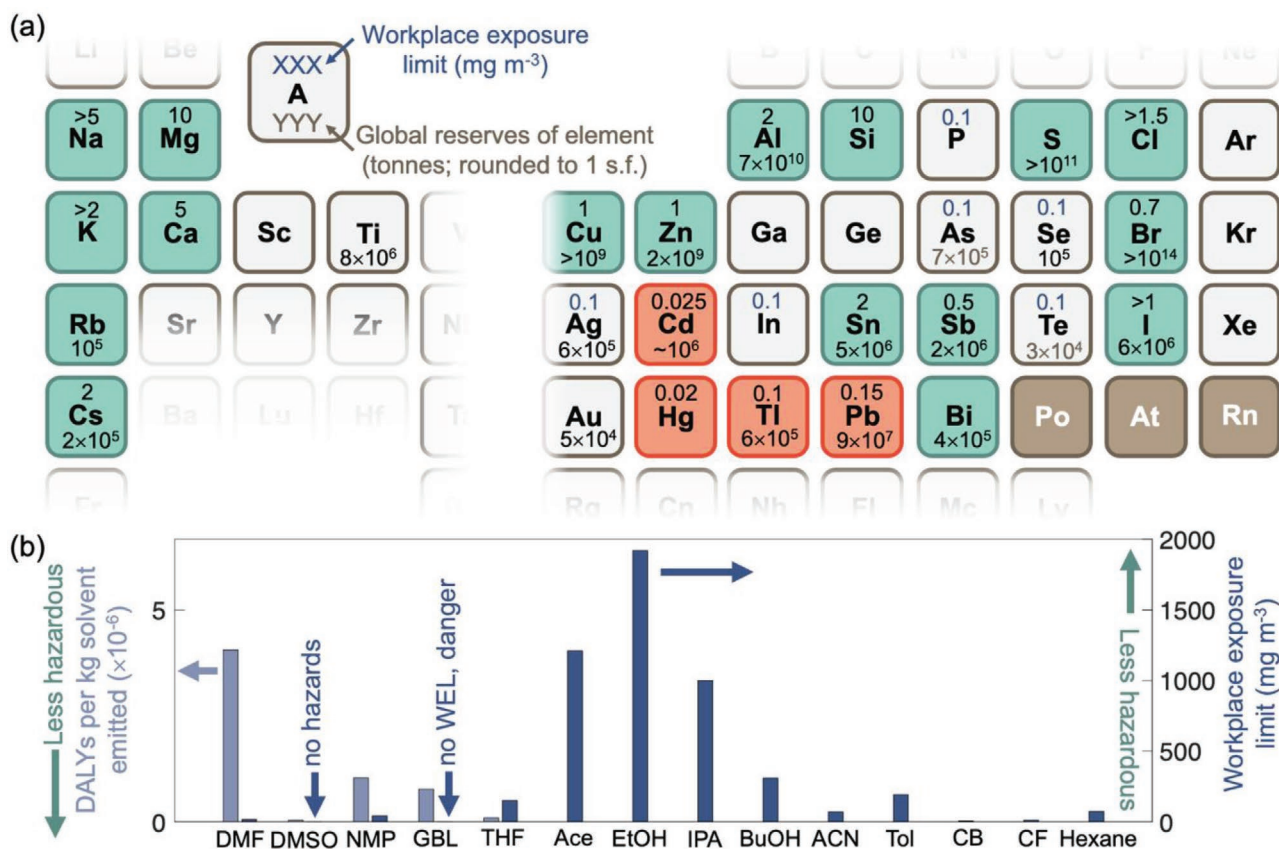
**ADVANCED
ENERGY
MATERIALS**

www.advenergymat.de

Figure 10. Sustainability of precursors for established, emerging, and potential inorganic indoor photovoltaic (IPV) materials. a) Toxicity and abundance of elements used in relevant solar absorbers. Workplace exposure limit for 8 h period obtained from Ref. [192] and [193]. Elements with a workplace exposure limit of ≥ 0.5 mg m^{-3} (or equivalent based on LD$_{50}$ data; Table S1, Supporting Information) are shaded green. Regulated toxic elements (Cd, Hg, Tl, and Pb) are shaded red. Radioactive elements are shaded brown. Elemental abundance data obtained from Ref. [190]. b) Toxicity of solvents, based on the disability-adjusted life years (DALYs[194]) and the 8 h workplace exposure limit.[193] Abbreviations: DMF (*N,N*-dimethylformamide), DMSO (dimethyl sulfoxide), NMP (1-methyl-2-pyrrolidinone), GBL (*γ*-butyrolactone), THF (tetrahydrofuran), Ace (acetone), EtOH (ethanol), IPA (propan-2-ol), BuOH (butan-2-ol), ACN (acetonitrile), Tol (toluene), CB (chlorobenzene), CF (chloroform). Hexane refers to *n*-hexane.

lighting (specifically, 1650 lx WLED lighting) using a bulk heterojunction between a polymer donor (PM6) and a small-molecule acceptor (Y6-O). Critically, an organic electron transport layer (PDI-NO) with a high highest occupied molecular orbital (HOMO) was used to more effectively block holes at the cathode and reduce leakage currents, giving higher efficiencies under low illumination levels.[14] The molecular structures are shown in Figure 8c, with the device structure shown in Figure 8g. In these devices, a $V_{oc} > 1$ V was achieved,[14] which exceeds the typical V_{oc} values previously achieved in a-Si:H, III–V and DSSC systems.[15,156]

Organic materials can be dissolved in a variety of solvents, and therefore benefit from compatibility with high-throughput roll-to-roll processes, as well as other solution-based methods (e.g., blade coating).[10,215] Historically, organic photovoltaics are based on bulk heterojunctions with fullerene-based acceptors.[213] However, these fullerene-based blends have suffered from light-induced degradation, high synthesis costs, and limited tunability in the energy levels of the fullerene acceptors.[216,217] Since 2015, however, there has been a resurgence in interest in nonfullerene acceptors, such as 3,9-bis(2-methylene-(3-(1,1-dicyanomethylene)-indanone))-5,5,11,11-tetrakis(4-

hexylphenyl)-dithieno[2,3-d:2′,3′-d′]-s-indaceno[1,2-b:5,6-b′]-dithiophene (ITIC).[218] Blends based on polymers and nonfullerene acceptors have demonstrated improved photostability, as well as increased efficiencies >17% under 1 sun illumination.[219] The operating lifetime of such blends has already been predicted to reach 11 yr under 1 sun illumination.[218] A recent study also reported a polymer blend with a nonfullerene acceptor derived from ITIC, finding no degradation in device performance under 1000 lx WLED lighting after 1000 h testing.[220] However, these measurements were made with the devices encapsulated,[220] and the stability of blends with nonfullerene acceptors against oxygen, moisture, heat and mechanical stress, as well as irradiation, needs to be fully elucidated.[214] In addition, analyses have found that ITIC and its derivatives have higher synthesis costs than PC$_{71}$BM,[218] which is already considered expensive.[214,216] It will therefore be important to develop alternative synthesis routes or explore materials with lower synthesis costs but high stability.

Owing to their processability at low temperatures from solution, organic photovoltaics have an energy payback time of only 0.3–0.5 yr for outdoor light harvesting,[189] which is significantly shorter than for a-Si:H and DSSCs (Sections 4.1

**ADVANCED
SCIENCE NEWS**

www.advancedsciencenews.com

**ADVANCED
ENERGY
MATERIALS**

www.advenergymat.de

and 4.2). Furthermore, as discussed above, organic photovoltaics are highly flexible in terms of the molecular structures of the materials and processing methods used. Life cycle analyses of devices with fullerene acceptors have shown that the cumulative energy demand of producing the entire device is dominated by the production of the fullerene component. Other large components of the cumulative energy demand are high-energy vacuum-based steps, such as the sputtering of the indium tin oxide (ITO) transparent electrode.[189,221–223] Thus, further reductions in the energy payback time and the cumulative energy demand associated with device manufacturing could be achieved by replacing ITO sputtering with screen printing of alternative electrodes, such as graphite.[189,224] Another important advantage of organic photovoltaics is the low toxicity of the materials. Current analyses have shown no evidence of organic photovoltaics posing an environmental threat in case of the release of the materials during catastrophic device failure or during decommissioning.[225] However, the solvents used during manufacturing (and potentially during recycling) also need to be taken into account. Common solvents include chlorobenzene and chloroform, which make a negligible contribution to the cumulative energy demand of the devices,[223] but which are toxic (Figure 10b). Developing manufacturing processes for organic photovoltaics using nontoxic solvents would therefore be desirable.[224]

4.4. Lead-Halide Perovskites

Lead-halide perovskites are a recent entry into the photovoltaics research scene. Perovskites refer to a family of ternary materials (general chemical formula of ABX_3), in which the B-site cations are octahedrally coordinated with X-site anions, and with A-site cations occupying the cuboctahedral cavities. A 3D symmetric crystal structure forms, usually with a cubic or tetragonal unit cell. In the case of LHPs, the B-site cation is Pb^{2+}, X-site anions a halide (I^-, Br^-, or Cl^-), and A-site a monovalent cation (e.g., $CH_3NH_3^+$) of the correct size to fit within the cuboctahedral voids and maintain the perovskite crystal structure (Figure 8d).[169,226–228] LHPs were first reported in photovoltaics in 2009 with a power conversion efficiency of 3.8% under 1 sun,[229] but rapidly rose in efficiency to reach a certified value of 25.5% in 2020.[230–232] The learning rate exhibited by LHP solar cells is unprecedented,[233] and these devices have rapidly surpassed the highest certified efficiencies of their thin-film counterparts to now be on the cusp of reaching the highest certified efficiency of single-junction c-Si (26.7%).[170,230] This trend has been replicated in IPV, with LHP photovoltaics rapidly surpassing a-Si:H, DSSC and organic photovoltaics to reach an efficiency of 37.2% under 1000 lx WLED lighting in 2020 (active device area of 0.10 cm^2).[13] This was achieved using an n–i–p device structure (Figure 8h), in which a bilayer of SnO_2 and ZnO nanoparticles were used as the electron transport layer. This bilayered structure was found to reduce the trap density at the interface between the perovskite and electron transport layer (as compared to using only SnO_2 for the electron transport layer), and therefore increase the V_{oc} to a value of 1.20 V under 1 sun (representing a V_{oc} loss of only 0.13 V) by reducing nonradiative recombination. As a result, there was only a small

reduction in the V_{oc} under low illumination levels, such that the V_{oc} of the IPV devices under 1000 lx WLED lighting was close to 1 V.[13] We note that these IPV were achieved using $MAPbI_3$, which has a sub-optimal bandgap of 1.6 eV (Figure 13b). The bandgap has been widened to 1.8 eV through anion alloying with Br and Cl.[234] This led to 36.2%-efficient IPV (with 0.10 cm^2 active device area) under 1000 lx FL lighting.[234] Although these devices are not yet as efficient as champion $MAPbI_3$ IPV, we should bear in mind that the halide perovskite IPV field is at an early stage in its development, and that efforts to fully address nonradiative recombination at interfaces and in the bulk of the absorber still need to be made.

However, a key challenge of LHPs is their limited photo-, thermal, and environmental stability. In particular, methylammonium lead iodide ($MAPbI_3$) is thermodynamically unstable,[235] and many degradation pathways involve methylammonium.[169] Thus, although current work on perovskite IPV has primarily focused on $MAPbI_3$,[153] more efforts should be made into LHPs with other A-site cations that have demonstrated improved stability (e.g., a mixture of Cs and formamidinium, or FA, in the A-site).[13,169] Another successful strategy to improve the stability of LHP devices is to incorporate moisture barriers, including highly dense oxide coatings (especially those grown by atomic layer deposition),[236–238] indium tin oxide,[239,240] as well as low-dimensional perovskite capping layers.[241–243] For example, Bush et al. demonstrated that Cs$_{0.17}$FA$_{0.83}$Pb(Br$_{0.17}$I$_{0.83}$)$_3$ solar cells with a SnO_2/zinc tin oxide overlayer, as well as an indium tin oxide transparent top electrode were stable for 1000 h under 1 sun illumination under ambient conditions (40% relative humidity on average).[240] Grancini et al. also demonstrated 1 yr (>10 000 h) device stability in $MAPbI_3$ covered with a 2D perovskite under 1 sun.[243] Packaging the LHP devices with glass and ethylene-vinyl acetate (which is used in packaging c-Si solar cells) has also been shown to allow the devices to be stable for 1000 h at 85 °C and 85% relative humidity,[169,240] although thinner packaging may be needed for IPV applications when integrated with small and wearable electronics. Beyond developing moisture barriers and packaging, it has been shown that controlling the interfaces between the perovskite and charge transport layers is critical for improving device stability.[244–246] Thus, despite the instability of $MAPbI_3$, several strategies have been shown to be successful in improving the stability of LHP photovoltaics, and techno-economic analyses of LHP solar cells have assumed that 15–20 yr module lifetimes are achievable in the future.[247,248]

Work on LHPs is entering into the commercial phase, with an increasing number of groups developing scalable routes to manufacturing perovskite solar cells. These include solution- (e.g., blade coating,[249] inkjet printing,[250] and rapid spray plasma processing[251]) and vapor-based methods (e.g., thermal evaporation,[252] chemical vapor deposition,[253] and vapor transport deposition[254]). Mini-modules with >10 cm^2 area have been achieved by solution-processing, thermal evaporation and chemical vapor deposition,[249,253,255,256] which may be sufficient for a wide range of IPV applications.[10] Perovskite mini-modules with 25 cm^2 area have also been demonstrated for IPV, with a power density of 89.4 µW cm^{-2} produced under 1000 lx FL lighting,[257,258] which would be sufficient for a wide range of wireless sensors.[10] It is projected that perovskite modules can

be manufactured by high-throughput solution-based methods with annual production on the order of 10^6 m^2 yr^{-1}, with a manufacturing cost of $ 0.01 cm^{-2} or lower, which would be highly competitive for IPV applications.[10,247]

LHP modules can be manufactured using similar processes as DSSCs and OPVs, and therefore also have lower cumulative energy demand than a-Si:H.[180,187–189,259] Combined with LHP devices giving higher efficiencies than DSSCs, OPVs, and a-Si:H, the energy payback time for LHP solar cells is <0.5 yr for outdoor light harvesting.[187] However, LHPs contain lead, which is a hazardous element (Figure 10a) that is regulated in markets worldwide. In particular, LHPs are water-soluble, making the lead component highly accessible in the event of a catastrophic failure of the device packaging. One of the widely followed lead regulations is the RoHS, which stipulates no more than 0.1 wt% lead in commercial products.[260] Although outdoor photovoltaics are exempt from these regulations, PV used indoors for consumer electronics are not. However, the RoHS defines the lead content based on a homogeneous product, and for PVs, this would include the substrate. Analyses have shown that whether LHP devices exceed this threshold depends in part on the substrate, in which thick glass substrates result in the lead content falling below the threshold of 0.1 wt% for the device, whereas thin flexible substrates would result in the lead content being above this threshold.[261] However, other jurisdictions have lower tolerances for lead,[261,262] and analyses have shown that lead from LHP devices can enter into the food cycle, where it would bioaccumulate.[263] It is therefore critical to mitigate the hazards associated with lead in LHPs, and some recently proposed solutions include using coatings that could sequester lead in the case of catastrophic device failure,[264] and the development of Fe-decorated hydroxyapatite that could extract lead from contaminated water.[265] Beyond lead, some of the solvents used to fabricate perovskite thin films are highly toxic. These include *N,N*-dimethylformamide (DMF), *γ*-butyrolactone (GBL), and 1-methyl-2-pyrrolidinone (NMP), which have low workplace exposure limits and are labeled as dangerous (Figure 10b). In a recent analysis, the disability-adjusted life years (DALYs) of common polar solvents used in LHP synthesis were calculated, which quantifies the sum of the years of life lost due to premature mortality or disability as a result of exposure to these solvents.[194] From Figure 10b, it can be seen that DMF, GBL, and NMP have the highest DALYs, whereas dimethylsulfoxide (DMSO) is significantly more benign. It should be noted that the quantity of solvents used in perovskite device manufacturing is low, resulting in the overall environmental impact being low despite the toxicity of the solvents.[194] However, future legislation may limit the use of toxic solvents, and developing green processing routes will be important for perovskite IPV.[194]

5. Potential of Emerging, Nontoxic Materials for Indoor Photovoltaics

From Section 4, it could be seen that while a-Si:H is one of the dominant materials in the IPV industry, DSSCs and OPVs are emerging alternatives that offer several advantages, namely increased efficiency and reduced energy payback time. LHPs

have rapidly surpassed the performance of all of these materials under indoor lighting, demonstrate lower energy payback times (calculated under outdoor lighting), and there are promising results that show that LHP modules can be manufactured cost-effectively at scale, with module lifetimes that will be sufficient for IPV applications. As such, companies have already appeared with the aim of commercializing LHP IPV.[262] The limitation of LHPs is their toxicity, both of the lead component (which is regulated in markets worldwide), and of the polar solvents that are currently popularly used. Finding alternative materials and processes that could replicate the exceptional performance of LHPs but without the same toxicity limitations is a key question in the field.

As a result, lead-free PIMs have gained substantial attention. Several approaches have been taken to develop PIMs, namely to identify 1) chemically analogous materials (e.g., tin-based perovskites, vacancy-ordered double and triple perovskites, or silver-bismuth-iodide rudorffites), 2) structurally analogous materials (e.g., halide double perovskites), or 3) electronically analogous materials (e.g., bismuth oxyiodide, BiOI, or binary halides). The third approach in particular aims to find materials that could replicate the defect tolerance of the LHPs, in which low nonradiative recombination rates are achieved despite high densities of defects, owing to shallow traps with low capture cross-sections.[142,274–276] The classes of materials explored and ideas for how defect tolerance arises are reviewed elsewhere.[169,226,277–283] However, nearly all efforts with PIMs thus far have been in outdoor light harvesting, where their performance so far has been low. The low performance is partly due to the wide bandgaps of the materials that are close to 2 eV in many cases. These bandgaps, however, are suitable for indoor light harvesting, and the potential of these materials for IPV was recently explored.[138] This section discusses the potential performance of PIMs for IPV.

5.1. Lead-Free, Layered Materials Explored for Indoor Photovoltaics

5.1.1. Bismuth Oxyiodide and Cesium Antimony Iodide-Chloride

Recently, we demonstrated the promise of two PIMs for IPV: BiOI and cesium antimony iodide-chloride ($Cs_3Sb_2I_{9-x}Cl_x$).[138] As shown in Figure 10a, bismuth- and antimony-based compounds have lower levels of toxicity than lead-based compounds. Antimony-based compounds have an 8 h workplace exposure limit of 0.5 mg m^{-3}, which is over three times larger than that of lead-based materials,[193] and antimony is not a restricted element in the RoHS directive.[285] Bismuth-based compounds have demonstrated very little evidence for toxicity, with bismuth known as the "green" element.[286] Furthermore, BiOI is grown by thermal chemical vapor deposition (t-CVD) using nonhazardous precursors (BiI$_3$ vapor and O$_2$/Ar gas).[266] $Cs_3Sb_2I_{9-x}Cl_x$ thin films are currently deposited from a solution of DMSO and DMF, with a toluene antisolvent. As discussed earlier and shown in Figure 10b, DMF is hazardous and alternative solvents may need to be developed in the future if this material is grown from solution at a large scale.

An appealing feature of BiOI and $Cs_3Sb_2I_{9-x}Cl_x$ is that they have a layered rather than 0D crystal structure (**Figure 11**a,b). Early work on PIMs focused on the first approach of finding
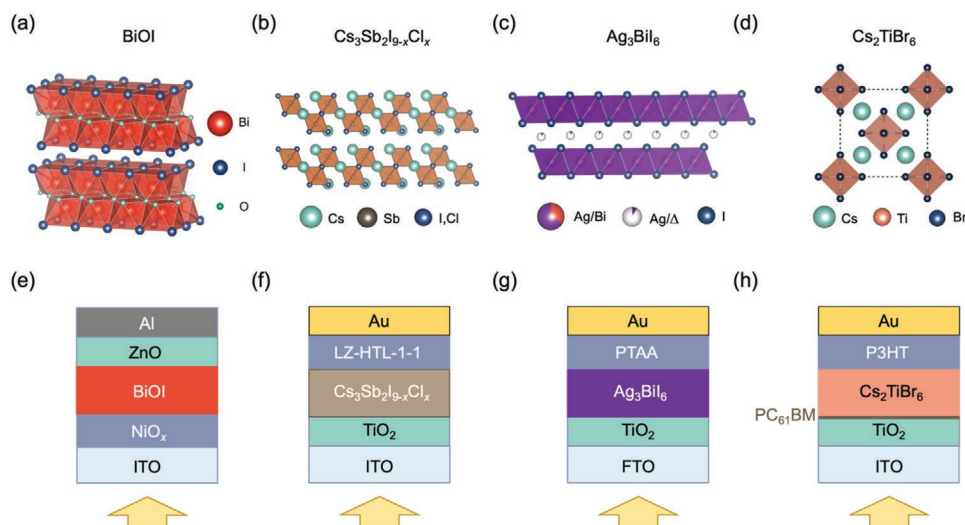
Figure 11. a–d) Crystal and e–h) device structure of perovskite-inspired materials with potential for indoor photovoltaics. a,e) bismuth oxyiodide, or BiOI, b,f) cesium antimony iodide–chloride, or $Cs_3Sb_2I_{9-x}Cl_x$, c,g) silver bismuth iodide, or Ag_3BiI_6, where Δ represents a vacancy, d,h) cesium titanium bromide vacancy-ordered double perovskite, or Cs_2TiBr_6. The device structures represent those that have given state-of-the-art efficiencies.[138,272,284]

chemically analogous materials to LHPs, such as $MA_3Bi_2I_9$, $Cs_3Bi_2I_9$, and $Cs_3Sb_2I_9$.[287–290] However, these vacancy-ordered triple perovskites (i.e., $A_3B_2X_9$ compounds) have a structural dimensionality close to 0D, with disconnected B_2X_9 groups (**Figure 12**a, left). Band dispersion is therefore low, effective masses high, and mobilities low in these materials.[275,287,291–293] In addition, the localization of charge carriers within the B_2X_9 groups results in high exciton binding energies of several hundred meV.[291,292,294,295] Collectively, the low mobilities and high exciton binding energies lead to low photoconversion efficiencies. However, $Cs_3Sb_2I_9$ can also exist in a 2D polymorph.[287]

It was found that this layered polymorph could be stabilized by alloying Cl atoms into the X-site (Figure 12a, right),[296,297] leading to an order-of-magnitude improvement in the Hall mobility from 0.5 cm^2 V^{-1} s^{-1} (0D) to 5.7 cm^2 V^{-1} s^{-1} (2D), which led to the power conversion efficiency also increasing by an order of magnitude.[297] BiOI also naturally forms a layered structure, and from fitting time-correlated single photon counting measurements, the mobility was estimated to be 14 cm^2 V^{-1} s^{-1}.[266] However, the mobility is highly anisotropic, and we recently showed that an a/b-axis preferred orientation could be achieved by controlling the growth temperature
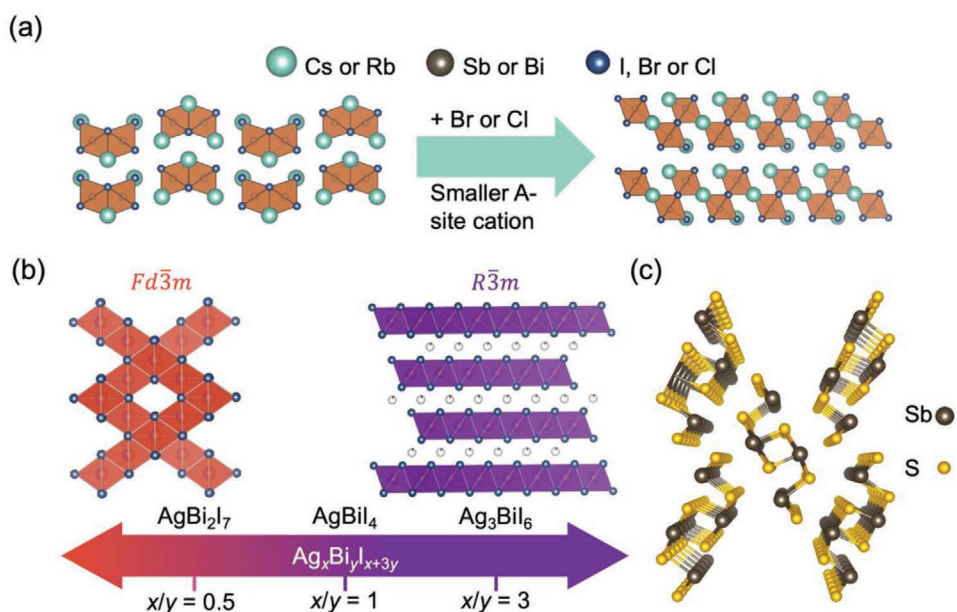

Figure 12. Crystal structures of a) $A_3B_2X_9$ vacancy-ordered triple perovskites, e.g., $Cs_3Sb_2I_9$ or $Rb_3Sb_2I_9$, showing how the structural dimensionality can be tuned through the A-site and halide species, b) silver iodobismuthates, showing how the crystal structure can be tuned from defect-spinel ($Fd\bar{3}m$) to layered ($R\bar{3}m$) through the x/y ratio, and c) 1D Sb_2S_3.
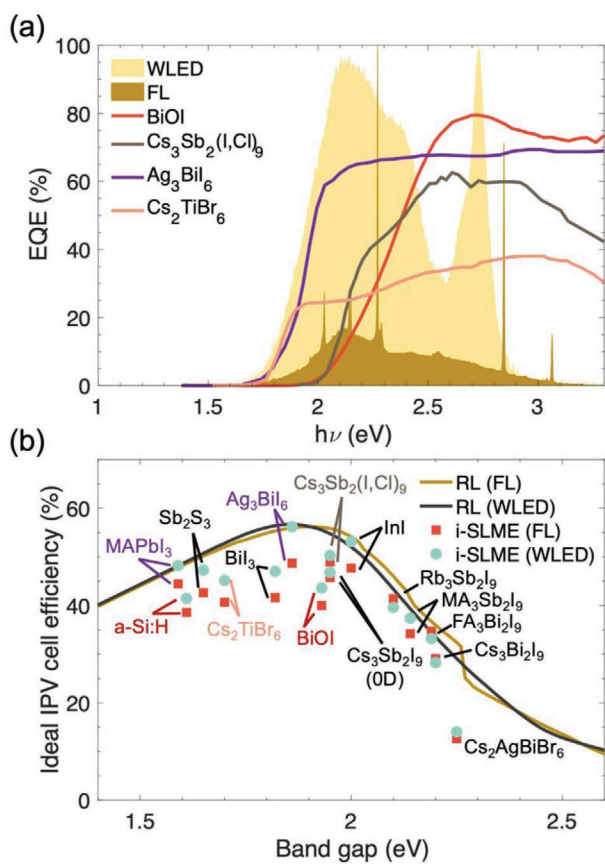
Figure 13. Performance and potential of perovskite-inspired materials for indoor photovoltaics. a) External quantum efficiency (EQE) spectra of the devices compared to the spectra for white light-emitting diode (WLED) and fluorescent light (FL) spectra. b) Indoor spectroscopic limited maximum efficiency (i-SLME) of various perovskite-inspired materials under WLED and FL spectra compared to the radiative limit (RL). Details of the calculations.[138] Further details.[178] Data for the EQE spectra in (a) (BiOI and $Cs_3Sb_2(I,Cl)_9$),[138] (Ag_3BiI_6),[284] (Cs_2TiBr_6).[272] The illumination spectra for (a) and the data for (b).[138]

during t-CVD growth, such that the high-mobility planes connected the top and bottom electrodes in the photovoltaic device stack.[298] As a result, external quantum efficiencies reaching up to 80% at 450 nm wavelength were achieved in BiOI devices.[268]

BiOI and $Cs_3Sb_2I_{9-x}Cl_x$ have bandgaps close to the optimum value of 1.9 eV,[297,268] and these bandgaps were found to be photostable.[138] The EQE spectra of devices made from both materials are closely matched with the indoor light spectra (**Figure 13**a). The optimal, photostable bandgaps of these materials are advantageous over $MAPbI_3$, which has a lower bandgap of 1.55 eV. The bandgap of $MAPbI_3$ can be increased by alloying with Br, however this is not photostable, and it has been shown that the photoluminescence peak of iodide-bromide perovskites will red-shift over time under illumination.[299]

To determine the ultimate efficiency potential of these materials, we calculated the indoor spectroscopic limited maximum efficiency (i-SLME), as shown in Figure 13b, and detailed in Tables 3 and 4. The i-SLME gives the power conversion efficiency that would be achieved if i) all absorbed photons give rise to free electron–hole pairs that are then all extracted into

the external circuit, and ii) the only nonradiative recombination comes about due to how close, energetically, the bandgap is to the first direct transition, i.e., that a direct bandgap material would be able to achieve a photoluminescence quantum efficiency of 100% (details in the footnote of Table 4).[300] The i-SLMEs shown in Figure 13b were calculated using the experimentally measured optical absorption coefficient, and assuming an absorber thickness of 500 nm. This provides a useful measure of the optically limited efficiency potential. However, materials may ultimately not reach the i-SLME for several reasons, such as: i) high exciton binding energies preventing photogenerated electron–hole pairs from being separated, ii) introduction of extra nonradiative recombination due to deep traps in the bulk or surface, or iii) disorder in the material giving rise to extra nonradiative losses due to high Urbach energies.[178] These factors therefore need to be considered when optimizing the crystal structure (influencing exciton binding energy) and processing (influencing traps present and Urbach energy) of new materials.

Owing to its high absorption coefficient and optimal bandgap, $Cs_3Sb_2I_{9-x}Cl_x$ was calculated to have an i-SLME of ≈50% (Figure 13b and Table 3), which is close to the radiative efficiency limit. However, BiOI was found to have a lower i-SLME of 40–44% (Figure 13b and Table 3), which is due to the lower absorption coefficient and shallower absorption onset. Nevertheless, BiOI has the advantages of being processable by a scalable t-CVD method at low temperatures of ≈350 °C,[268,298,301] as well as the thin films being stable in ambient air without encapsulation for at least 197 days[268] (whereas $MAPbI_3$ thin films degrade within 5 days in the same conditions).[290] Both BiOI and $Cs_3Sb_2I_{9-x}Cl_x$ IPVs were found to be stable for several months when stored inside a glovebox with >1000 ppm O_2 and >500 ppm H_2O.[138] Both materials therefore hold promise for delivering stable performance and have the potential of being manufacturable at scale in the future. Furthermore, the abundance of Bi, Sb, I, Cl and Cs are at least an order of magnitude larger than that of Te (Figure 10a). Since Te is already used commercially in CdTe solar cells, we would expect that the abundance of the elements used in BiOI and $Cs_3Sb_2I_{9-x}Cl_x$ IPVs to be sufficient for commercialization.

We characterized the performance of BiOI and $Cs_3Sb_2I_{9-x}Cl_x$ IPV under 1000 lx WLED and FL lighting (device structures shown in Figure 11e,f), and found the efficiencies to be within the 4–5% range, in which the active device areas were 0.0725 cm². This first demonstration of PIMs for IPV is therefore already within the range of efficiencies demonstrated by commercial a-Si:H IPV (refer to the introductory paragraph of Section 4). We showed that both BiOI and $Cs_3Sb_2I_{9-x}Cl_x$ IPV, with 7.25 mm² device area, were already sufficient for powering carbon nanotube inverters under indoor lighting, with a gain >7 V V⁻¹, which would be adequate for robust digital signal processing.[138] Furthermore, we found that there is significant scope for further improvements in IPV efficiency. Firstly, the devices we used had 1 sun efficiencies close to the median efficiencies for these materials, which were approximately half of our previously published record values.[138,297,268] Further optimization within the current device structure is therefore likely to deliver performance improvements to the IPVs. Secondly, our device and optical loss analyses showed that the

ADVANCED
SCIENCE NEWS
www.advancedsciencenews.com

ADVANCED
ENERGY
MATERIALS
www.advenergymat.de

main loss mechanism in both devices was due to uncollected photo-generated carriers. In BiOI, this is likely due to non-radiative recombination resulting from the downward band bending of BiOI next to the nickel oxide hole transport layer.[268] In $Cs_3Sb_2I_{9-x}Cl_x$, on the other hand, the discontinuous morphology is likely limiting the efficiency.[138] Both limiting factors can be addressed by optimizing the charge transport layers used, as well as the processing of the absorber layer.

Thus, BiOI and $Cs_3Sb_2I_{9-x}Cl_x$ have given promising first results for their applications in IPV. In particular, they could overcome the stability and toxicity limitations of the LHPs, while having the potential to reach high efficiencies in the future. Both materials are processed at relatively low temperatures. BiOI is grown by t-CVD, which is already scalable. Although $Cs_3Sb_2I_{9-x}Cl_x$ is currently grown by spin-coating, it has the potential to be compatible with large-area solution-based methods (as previous works on LHPs and OPVs have shown). All constituent elements in BiOI and $Cs_3Sb_2I_{9-x}Cl_x$ are sufficiently abundant for commercialization and are not subject to legal restrictions. These materials therefore have the potential to be manufactured cost-effectively at scale and used commercially.

5.1.2. Tin-Based Perovskites

Tin-based perovskites have also recently been reported for IPV. Tin-based perovskites retain the 3D structural dimensionality of $MAPbI_3$, and therefore benefit from high mobilities and low exciton binding energies.[303,304] In addition, substituting Pb^{2+} with Sn^{2+} in the halide perovskite structure leads to a reduction in the bandgap, owing to the higher energies of the valence cation s orbitals that are closer to the halide 5p orbital, giving rise to strong splitting in the bonding-antibonding states.[305] Thus, $MASnI_3$ has a bandgap of 1.3 eV,[306] which is close to the optimum value for absorbing AM 1.5G radiation. These favorable properties, as well as the significant attention the tin-based perovskites have attracted in the community, have contributed to tin-based perovskites demonstrating the highest 1 sun PCEs amongst all lead-free perovskite-inspired materials,[279] with values up to 12.4% reported for $PEA_{0.15}FA_{0.85}SnI_3$ (where PEA is phenethylammonium; FA is formamidinium).[307] Indeed, Yang et al. recently reported a $FA_{0.75}MA_{0.25}SnI_2Br$ perovskite, doped with 1% Catechin (flavan-3-ol), that achieved 12.81% efficiency under 1000 lx indoor lighting (active device area of 0.0725 cm^2).[268] These devices were 6.02%-efficient under 1 sun illumination,[268] and there is therefore potential for future efficiency improvements, even by simply using other tin-based perovskite compositions and device structures that have already delivered higher 1 sun efficiencies. However, the low bandgap of 1.3 eV restricts the efficiency potential, with a radiative limit of only 36% under 1000 lx FL or WLED lighting (Figure 13b). This is lower than the 40–50% i-SLME values for $MAPbI_3$, BiOI and $Cs_3Sb_2I_{9-x}Cl_x$ (Figure 13b and Table 3). Thus, future work should focus on developing tin-based perovskites with bandgaps that are wider (closer to 1.9 eV), but which are also photostable.

Originally, tin-based perovskites had low stability in air, along with the facile oxidation of Sn^{2+} to Sn^{4+} and high p-type doping.[268,303,304] However, extensive efforts have been made to address this (e.g., through doping with SnF_2 or Catechin), and devices that are stable in air without encapsulation have now been achieved.[268,303,304,308]

Another feature of tin-based perovskites that has attracted groups to work on this family of materials is the potential for low toxicity. This was recently examined in detail by Babayigit et al. Although they found that tin-based perovskites could pose a greater toxicity risk than lead-based perovskites, this was due to the HI evolved from the SnI_2 decomposition product. The tin cation itself did not pose a significant risk because it readily oxidized to form metal oxides based on Sn^{4+}.[267] It is therefore believed that the toxicity risks of tin-based perovskites could be mitigated, since the HI decomposition products are likely to degrade or be diluted if released to the environment.[309] However, a risk associated with the manufacturing of tin-based perovskites would be the toxicity of the solvents currently being used, which are often the same as for LHPs. Thus, as with LHPs, future efforts to scale up the manufacturing of tin-based perovskites via solution-based routes should develop processes based on low-toxicity solvents.

5.2. Future Perovskite-Inspired Materials

The analysis in Figure 13b shows that the wider PIMs family also has significant potential for IPV. Comparing with Figure 10a shows that many of these materials are composed of low-toxicity elements that are sufficiently abundant for commercialization. Although these materials have only been considered for outdoor PV applications, efforts should be made to consider these materials for IPV, given that their bandgaps are close to the optimal 1.9 eV value for IPV, whereas their efficiencies under 1 sun illumination would always be limited by their wide bandgap. Two of the materials are Ag_3BiI_6 rudorffites and Cs_2TiBr_6 vacancy-ordered double perovskites (crystal structures shown in Figure 11c,d).

5.2.1. Silver Iodobismuthate Rudorffites

Silver-bismuth-iodide compounds (or silver iodobismuthates) have the general formula: $Ag_xBi_yI_{x+3y}$, and are comprised of edge-sharing AgI_6 and BiI_6 octahedra, coordinated with vacancies in the cation sites (denoted Δ) depending on the value of x.[284,310,311] The prototypical oxide for this family of iodobismuthates is $NaVO_2$, which was discovered by Rüdorff and Becker in 1954.[312] Given that perovskites were named after Lev Perovski,[313] Turkevych et al. proposed to name the silver iodobismuthate family of materials rudorffites,[284] and this has gained traction in the field. The silver-bismuth-iodide rudorffites have been reported to adopt either a 3D cubic defect-spinel structure with vacant tetrahedral sites (space group: $Fd\bar{3}m$), or a layered rhombohedral structure (space group: $R\bar{3}m$), as illustrated in Figure 12b.[284,310] The structure adopted depends on the composition. $AgBiI_4$ was found to exist in either the $Fd\bar{3}m$ or $R\bar{3}m$ structure,[314] whereas compounds with $x/y > 1$ (e.g., Ag_3BiI_6 and Ag_2BiI_5) favor the $R\bar{3}m$ phase and compounds with $x/y < 1$ (e.g., $AgBi_2I_7$) favor the $Fd\bar{3}m$

**ADVANCED
SCIENCE NEWS**

www.advancedsciencenews.com

**ADVANCED
ENERGY
MATERIALS**

www.advenergymat.de

phase.[284,310] The bandgaps for these materials were reported to be in the 1.63–1.90 eV range.[284,310,311,314–316] In particular, the Ag-rich compound Ag_3BiI_6 has a bandgap close to the optimum for indoor light harvesting (1.83–1.89 eV),[310] along with high absorption coefficients of ≈10^5 cm^{-1} near the band-edge.[310] This material therefore has the highest calculated i-SLMEs of 56.2% (1000 lx WLED) and 48.7% (1000 lx FL); refer to Table 3. These are the highest i-SLMEs for the PIMs analyzed in Figure 13b. Furthermore, Ag_3BiI_6 has yielded the highest 1 sun solar cell efficiencies among the rudorffites, with power conversion efficiencies of 4.3% (device structure given in Figure 11g, with an active area of 0.25 cm^2).[284] Very recently, the related compound $AgBiI_4$ was demonstrated in IPV (0.04 cm^2 active device area), with 5.17% power conversion efficiency under 1000 lx WLED lighting that produced 1.76 µW cm^{-2} power.[273]

Another appealing feature of the silver bismuth iodide rudorffites is their lower toxicity compared to LHPs and improved stability. As discussed earlier, bismuth is a nontoxic element and iodine has a workplace exposure limit >1 mg m^{-3} (Figure 10a). Silver has an 8 h workplace exposure limit of 0.1 mg m^{-3}, which is lower than that for lead-based compounds (Figure 10a). While silver cations are highly toxic, solid silver-based compounds are substantially less toxic. Silver also bio-accumulates in algae, but current literature suggests that the silver absorbed by algae is nontoxic, and biomagnification of silver up the food chain is thought to be unlikely, which contrasts to lead.[317] Therefore, the ultimate toxicity and ecotoxicity of silver bismuth iodide rudorffites will depend on the decomposition products formed.

Groups have also reported the rudorffites to demonstrate improved stability compared to MAPbI$_3$. For example, Kim et al. reported both $AgBi_2I_7$ solar cells and thin films to be stable for 10 days under ambient conditions.[316] Sansom et al. reported $AgBiI_4$ to be structurally stable at up to 90 °C (whereas MAPbI$_3$ would degrade at 85 °C).[314] For Ag_3BiI_6 PVs, Pai et al. found the devices to retain >90% of the initial efficiency under 1 sun illumination after storing in ambient air (40% relative humidity) for 45 days.[269] At the same time, the stability of the silver bismuth iodide rudorffites does not appear to be as high as BiOI. Crovetto et al. reported a visual comparison of BiOI and Ag_3BiI_6, with Ag_3BiI_6 changing in color within a week while BiOI exhibited no visual change after several months of storage in ambient conditions.[310] Sansom et al. also reported that $AgBiI_4$ decomposed partially to AgI after 144 min of exposure to AM 1.5G radiation in air.[314] Furthermore, the activation energy barrier to Ag$^+$ migration in $AgBiI_4$ was reported to be only 0.44 eV,[318] which is similar to that for I migration in MAPbI$_3$,[319] suggesting facile ion migration.

In terms of scalability and manufacturability, silver bismuth iodide rudorffites have demonstrated versatility in the synthesis routes, which include solution processing and thermal evaporation. For solution processing, the approach and solvents used are similar to LHPs and other halide PIMs (i.e., spin-coating from a DMSO:DMF solvent).[316,320] Thus, the same challenges in developing processing routes with nontoxic solvents are needed (Sections 4.4 and 5.1). In thermal evaporation, it was demonstrated that the composition and phase of the materials grown can be controlled through the evaporation rates of the AgI and BiI$_3$ precursors.[311]

Thus, silver bismuth iodide rudorffites demonstrate promise owing to their bandgaps being close to the optimum for indoor light harvesting, along with the high absorption coefficients near their absorption onsets, leading to i-SLMEs close to the maximum RL of 57%. The toxicity of these materials is lower than in LHPs, but concerns over the silver component would need to be addressed in the future. The stability of these materials, while improved over MAPbI$_3$, may not be as high as BiOI. Nevertheless, the rudorffites are highly versatile materials with a wide range of available synthesis routes, and are therefore likely to be compatible with large-area deposition methods.

5.2.2. Cesium Titanium Bromide Vacancy-Ordered Double Perovskite

Double perovskites, or elpasolites, have the general formula: $A_2B'B''X_6$, where A is a monovalent cation, B' and B'' are metal cations and X an anion.[321,322] Examples include $Cs_2AgBiBr_6$, which gained interest owing to the long charge-carrier lifetimes >600 ns.[322,323] In particular, in double perovskites, the toxic lead cation can be substituted for two lower toxicity cations without compromising the 3D symmetric perovskite crystal structure. However, owing to the low electronic dimensionality, the bandgap is wide and indirect in many cases, resulting in low power conversion efficiencies. $Cs_2AgBiBr_6$ thin films have a bandgap of 2.25 eV as well as a low absorption coefficient <10^4 cm^{-1} near the band-edge owing to the indirect bandgap,[324] and therefore have i-SLMEs <20% (Figure 13b). Thus, in the best-case scenario in which all absorbed photons in $Cs_2AgBiBr_6$ are collected and no recombination centers are present, $Cs_2AgBiBr_6$ IPVs would not match the performance of DSSCs or OPV (refer to Sections 4.2 and 4.3).

A variation on the double perovskite family is to have a vacancy occupying one of the B-site cations, giving a vacancy-ordered double perovskite, with the general formula $A_2B(IV)X_6$, in which B(IV) is a tetravalent cation. The crystal structure is shown in Figure 11d. Although the structural dimensionality is 0D, the electronic dimensionality is higher owing to the close-packed halide sub-lattice, which gives rise to lower effective masses, especially in the valence band maximum.[325,326] One example is Cs_2TiBr_6, which has so far delivered the most efficient vacancy-ordered double perovskite solar cells (3.3% power conversion efficiency under 1 sun;[272] device structure shown in Figure 11h). The bandgap of this material is reported to be 1.78–1.82 eV,[271,272] and the absorption coefficient rapidly increases to the order of 10^5 cm^{-1} near the absorption onset.[272] As such, a high i-SLME of 45% is calculated under 1000 lx WLED lighting (Figure 13b).

Cs_2TiBr_6 is also a lower toxicity material than LHPs. Both Cs and Br have high workplace exposure limits (Figure 10a). Like Ag, the toxicity of Ti depends on the form it is in: while Ti is pyrophoric, TiO$_2$ is a benign compound with a workplace exposure limit of 10 mg m^{-3}.[193] TiBr$_4$, which is a precursor used in the growth of Cs_2TiBr_6,[272,327] decomposes to form HBr and TiO$_2$ in the presence of moist air or water. HBr has a 15 min workplace exposure limit of 10 mg m^{-3}.[193] While HBr is corrosive, it is likely generated in low quantities if evolved from TiBr$_4$ precursors, and this vacancy-ordered double perovskite material

ADVANCED
SCIENCE NEWS
www.advancedsciencenews.com

ADVANCED
ENERGY
MATERIALS
www.advenergymat.de

may therefore pose less of a safety risk than silver bismuth iodide rudorffites. Furthermore, Cs, Ti and Br are all abundant elements (Figure 10a). However, in terms of stability, there are conflicting reports. Chen et al. reported that Cs_2TiBr_6 is not susceptible to decomposing to form TiO_2 in the presence of moist air, and the devices retained 94% of their efficiency when stored for 14 days at 70 °C, 30% relative humidity and under ambient lighting.[272] By contrast, Euvrard et al. reported that Cs_2TiBr_6 powders decomposed to CsBr after 20 h of storage in an ambient environment.[271] Further investigation into the thermal, photo-, and environmental stability of Cs_2TiBr_6 is needed. Further efforts are also needed to expand upon the synthesis routes for growing Cs_2TiBr_6 thin films beyond the thermal evaporation route developed by Chen et al.,[272] since many reports thus far have focused on powders.[271,326,327]

5.2.3. Other Promising PIMs for IPV

Beyond silver bismuth iodide rudorffites and Cs_2TiBr_6, Figure 12b shows that high i-SLMEs >40% are achieved with BiI_3, InI, $Rb_3Sb_2I_9$ and Sb_2S_3. However, BiI_3 and InI have delivered low efficiencies of <2% under 1 sun illumination.[328,329] Furthermore, defect calculations have shown BiI_3 to have deep transition levels from defects with low formation energy (e.g., iodine and bismuth vacancies).[277] InI is predicted to have shallow traps,[277] but InI thin films grown by thermal evaporation have exhibited only weak photoluminescence[329] and In is not stable in the 1+ oxidation state, making the growth of phase-pure InI (as opposed to InI_3) challenging.

$Rb_3Sb_2I_9$ holds more promise. All elements are in their stable oxidation states, all are abundant and have high workplace exposure limits or LD_{50} values (Figure 10a; Table S1, Supporting Information). Furthermore, $Rb_3Sb_2I_9$ thin films have been reported to be stable in ambient air for at least 18 h, and photovoltaic devices stable for 150 days, retaining 84% of the original efficiency.[330] Furthermore, $Rb_3Sb_2I_9$ has a layered structure owing to the small size of the A-site cation, which leads to the 2D crystal structure being favored over the 0D structure (Figure 12a). The higher structural dimensionality leads to an exciton binding energy of 107 ± 10 meV, which is low compared to its 0D-structured vacancy-ordered triple perovskite (i.e., $A_3B_2X_9$) counterparts.[292] The bandgap is also direct, with a size of 2.03 eV,[292,330,331] and the i-SLME is 46% under 1000 lx FL lighting (Figure 12b). However, currently $Rb_3Sb_2I_9$ devices have efficiencies of up to ≈1.35% under 1 sun illumination,[330,331] and more work is needed to determine the limiting factors that need to be overcome to improve the performance.

On the other hand, Sb_2S_3 thin films have demonstrated higher efficiencies of up to 7.5% under 1 sun illumination.[332,333] These materials have 1D crystal structures (Figure 12c), and can be grown by scalable vapor-based methods, as well as solution-based methods,[332,333] and are composed of nontoxic, abundant elements (Figure 10a; Table S1, Supporting Information). However, although the i-SLME calculated from the absorption coefficients was 47% under 1000 lx WLED lighting (Figure 13b), Sb_2S_3 was found to form self-trapped excitons, which limited the maximum achievable efficiency by introducing an irreversible loss channel that limits the V_{oc}.[334] However, given the

high efficiencies already achieved, it is likely that Sb_2S_3 IPV will demonstrate efficiencies >10%. Coupled with the stability of Sb_2S_3 in air,[333,335] this material has potential for future exploration in indoor light harvesting.

6. Conclusions and Future Challenges to Realizing Sustainable Indoor Photovoltaics to Power IoT Devices

For the IoT to fulfill its promise to provide our daily objects and environments with "intelligence" and connectivity, it is essential to overcome the sustainability and technical challenges associated with the use of batteries as the sole power supplies of the IoT devices as the IoT ecosystem proceeds to one trillion nodes. A solution can be found in the use of compact energy harvesters, which tap energy freely available from the environment or human sources. At a functional level, in addition to allowing the efficient conversion of ambient energy, the ideal energy harvesting technology should be application-agnostic (i.e., widely deployable) and reliable. Given that a large number of IoT nodes are to be placed indoors, the deployability and reliability requirements point to the great appeal of indoor photovoltaics. Indeed, indoor light constitutes a predictable and controllable energy source; hence, it would enable the design of robust power management protocols toward the perpetual operation of the IoT nodes. Additionally, while indoor photovoltaics shares the attributes of deployability and reliability with ambient RF energy harvesting, it can deliver much higher power densities, which is attractive to meet the demands of more power-hungry IoT nodes as well as for the miniaturization of the corresponding devices.

In addition to functional requirements, energy harvesting technologies for the IoT need to deliver solutions that are environmentally sustainable, durable, and low cost. While durability and low cost are general requirements for a wide range of technologies, environmental sustainability is a particularly critical requirement for IoT applications, not only due to the sheer size of the IoT ecosystem, but also because of the typical placement of the IoT nodes in the vicinity of human end-users and the inherent challenges associated with recycling programs involving consumer electronic devices.

While the current commercial standard for IPV, hydrogenated amorphous silicon, is limited by its low performance, a wide range of alternatives have been developed that have potential to overcome these limitations and fulfill all requirements for IoT EHs. DSSC, OPV and LHP materials meet the requirements of efficiency and scalability. But future efforts with DSSCs will need to focus on achieving sensitizers and electrolytes for durable, cost-effective, and efficient devices that are also sustainable. One example is developing stable and low-cost solid-state electrolytes that can be synthesized using simple routes. Future efforts with OPV would need to improve the durability of the materials against moisture, oxygen, heat mechanical stress and irradiation, as well as explore low-cost nonfullerene acceptors, without compromising on their performance. LHPs benefit from low-cost

and comparatively simple fabrication routes, and promising developments are being made to improve their durability. However, their greatest challenge is in the toxicity of the lead component, as well as the toxicity of the solvents used in their fabrication. Efforts are already being made to mitigate these toxicity limitations, such as by developing solvent-free growth methods and coatings that can sequester lead. However, questions remain over whether lead-based perovskites can be commercially adopted for consumer electronics. Lead-free PIMs have demonstrated highly promising initial results, particularly in terms of their durability. Future efforts will need to focus both on improving the performance of the materials already investigated for IPV (e.g., by eliminating sub-optimal band alignments in BiOI device stacks and improving the film morphology in $Cs_3Sb_2I_{9-x}Cl_x$ devices), as well as exploring other promising PIMs. These include the PIMs identified in this Progress Report with potential for efficient, stable performance (namely silver iodobismuthates, $Rb_3Sb_2I_9$, Cs_2TiBr_6, and Sb_2S_3), as well as taking a more systematic approach to exploring the wider family of PIMs. This will involve making use of new understanding of what makes $MAPbI_3$ work so well (e.g., defect tolerance),[279] applying this understanding to design lead-free alternatives, gaining experimental insight into their defect properties and their relation to different processing strategies,[142] and using i-SLME calculations to identify the potential of these new materials for IPV applications at an early stage in their development. Critically, these efforts should focus on developing fabrication routes that either use green solvents or are solvent-free, as well as demonstrating the applicability of these new IPV in powering IoT electronics. Fully addressing these open technological questions could deliver a sustainable route to power the continued growth of the IoT ecosystem.

Supporting Information

Supporting Information is available from the Wiley Online Library or from the author.

Acknowledgements

Conflict of Interest

The authors declare no conflict of interest.

[1] K. Schwab, The Fourth Industrial Revolution: what it means, how to respond, https://www.weforum.org/agenda/2016/01/the-fourth-industrial-revolution-what-it-means-and-how-to-respond/ (accessed: January 2016).

[2] V. Tsiatsis, S. Karnouskos, J. Höller, D. Boyle, C. Mulligan, *Internet of Things*, Elsevier, London, UK **2019**.

[3] Q. Hassan (Ed.), *Internet of Things A to Z*, John Wiley & Sons, Inc., Hoboken, NJ **2018**.

[4] J. Davies, C. Fortuna (Eds.), *The Internet of Things*, Wiley, Hoboken, NJ **2020**.

[5] Forbes, IoT: number of connected devices worldwide 2012–2025, https://www.statista.com/statistics/471264/iot-number-of-connected-devices-worldwide/ (accessed: February 2021).

[6] H. Michaels, M. Rinderle, R. Freitag, I. Benesperi, T. Edvinsson, R. Socher, A. Gagliardi, M. Freitag, *Chem. Sci.* **2020**, *11*, 2895.

[7] Internet of Things (IoT) Market Worth $1319.08 Billion, Globally, by 2026 at 25.68% CAGR: Verified Market Research, https://www.prnewswire.com/news-releases/internet-of-things-iot-market-worth-1319-08-billion-globally-by-2026-at-25-68-cagr-verified-market-research-301092982.html (accessed: February 2021).

[8] Fin Capital, Forecast end-user spending on IoT solutions worldwide from 2017–2025, https://www.statista.com/statistics/976313/global-iot-market-size/ (accessed: February 2021).

[9] Wireless sensors: technologies and global markets, https://www.bccresearch.com/market-research/instrumentation-and-sensors/wireless-sensors-technologies-report.html (accessed: February 2021).

[10] I. Mathews, S. N. Kantareddy, T. Buonassisi, I. M. Peters, *Joule* **2019**, *3*, 1415.

[11] P. Harrop, Battery Elimination in Electronics and Electrical Engineering 2018–2028, **2018**.

[12] A. Keshavarzi, W. Van Den Hoek, *IEEE Des. Test* **2019**, *36*, 41.

[13] Y. W. Noh, I. S. Jin, K. S. Kim, S. H. Park, J. W. Jung, *J. Mater. Chem. A* **2020**, *8*, 17163.

[14] L. K. Ma, Y. Chen, P. C. Y. Chow, G. Zhang, J. Huang, C. Ma, J. Zhang, H. Yin, A. M. Hong Cheung, K. S. Wong, S. K. So, H. Yan, *Joule* **2020**, *4*, 1486.

[15] Y. Cao, Y. Liu, S. M. Zakeeruddin, A. Hagfeldt, M. Grätzel, *Joule* **2018**, *2*, 1108.

[16] E. Crenna, M. Secchi, L. Benini, S. Sala, *Int. J. Life Cycle Assess.* **2019**, *24*, 1851.

[17] G. Meijer, M. Pertijs, K. Makinwa (Eds.), *Smart Sensor Systems*, John Wiley & Sons, Ltd, Chichester, UK **2014**.

[18] D. Chew, *The Wireless Internet of Things*, John Wiley & Sons, Inc., Hoboken, NJ **2018**.

[19] R. Cheour, S. Khriji, M. Abid, O. Kanoun, in *2020 IEEE 6th World Forum Internet Things*, IEEE, Piscataway **2020**, pp. 1–7.

[20] T. Adegbija, A. Rogacs, C. Patel, A. Gordon-Ross, *IEEE Trans. Comput. Des. Integr. Circuits Syst.* **2018**, *37*, 7.

[21] M. Bolić, D. Simplot-Ryl, I. Stojmenović (Eds.), *RFID Systems*, John Wiley & Sons, Ltd, Chichester, UK **2010**.

[22] H. Qin, W. Zhang, *IEEE Trans. Mob. Comput.* **2014**, *13*, 2933.

[23] J.-H. Chen, Y.-S. Chen, Y.-L. Jiang, *IEEE Sens. J.* **2018**, *18*, 849.

[24] A. Gupta, T. Tsai, D. Rueb, M. Yamaji, P. Middleton, *Gartner Research Forecast: Internet of Things—Endpoints and Associated Services, Worldwide, 2017*, Gartner, Stamford, CT **2017**.

[25] P. Sparks, *The Route to a Trillion Devices*, ARM, Cambridge, UK **2017**.

[26] A. Holst, Global IoT End-User Spending Worldwide 2017–2025, **2021**.

[27] MarketsandMarkets Research Private Ltd., *Smart Sensor Market by Type (Temperature & Humidity, Pressure, Touch, Motion & Occupancy, Water, Position, Light, and Others), Technology (MEMS, CMOS), Component (ADC, DAC, Microcontroller), Connectivity, Industry, and Region – Global Forecast to 2025*, MarketsandMarkets Research Private Ltd, Northbrook, IL **2020**.

[28] S.-H. Yang, *Wireless Sensor Networks*, Springer, London **2014**.

[29] F. K. Shaikh, S. Zeadally, *Renewable Sustainable Energy Rev.* **2016**, *55*, 1041.

[30] A. Raj, D. Steingart, *J. Electrochem. Soc.* **2018**, *165*, B3130.

[31] L. Wang, Z. Wu, J. Zou, P. Gao, X. Niu, H. Li, L. Chen, *Joule* **2019**, *3*, 2086.

[32] K. (Kelvin) Fu, Y. Gong, G. T. Hitz, D. W. McOwen, Y. Li, S. Xu, Y. Wen, L. Zhang, C. Wang, G. Pastel, J. Dai, B. Liu, H. Xie, Y. Yao, E. D. Wachsman, L. Hu, *Energy Environ. Sci.* **2017**, *10*, 1568.

[33] Y. Shi, B. Li, Y. Zhang, Y. Cui, Z. Cao, Z. Du, J. Gu, K. Shen, S. Yang, *Adv. Energy Mater.* **2021**, *11*, 2003663.

[34] *Overcoming the Battery Obstacle to Ubiquitous Sensing—Finally: Why Self-Powered Sensors Are the Game-Changer*, Everactive Inc., Santa Clara, CA **2019**.

[35] E. Mossali, N. Picone, L. Gentilini, O. Rodrìguez, J. M. Pérez, M. Colledani, *J. Environ. Manage.* **2020**, *264*, 110500.

[36] MarketsandMarkets Research Private Ltd., *Battery Market for IoT by Type, Rechargeability, End-Use Application, and Geography – Global Forecast to 2025*, MarketsandMarkets Research Private Ltd, Northbrook, IL, **2020**.

[37] S. Davidsson Kurland, *Environ. Res. Commun.* **2019**, *2*, 012001.

[38] J. F. Peters, M. Baumann, B. Zimmermann, J. Braun, M. Weil, *Renewable Sustainable Energy Rev.* **2017**, *67*, 491.

[39] L. Gaines, K. Richa, J. Spangenberger, *MRS Energy Sustainability* **2018**, *5*, 12.

[40] G. Zubi, R. Dufo-López, M. Carvalho, G. Pasaoglu, *Renewable Sustainable Energy Rev.* **2018**, *89*, 292.

[41] S. Dühnen, J. Betz, M. Kolek, R. Schmuch, M. Winter, T. Placke, *Small Methods* **2020**, *4*, 2000039.

[42] D. Larcher, J.-M. Tarascon, *Nat. Chem.* **2015**, *7*, 19.

[43] S. Sudevalayam, P. Kulkarni, *IEEE Commun. Surv. Tutorials* **2011**, *13*, 443.

[44] K. S. Adu-Manu, N. Adam, C. Tapparello, H. Ayatollahi, W. Heinzelman, *ACM Trans. Sens. Networks* **2018**, *14*, 1.

[45] N. S. Hudak, G. G. Amatucci, *J. Appl. Phys.* **2008**, *103*, 101301.

[46] Poonam, K. Sharma , A. Arora, S. K. Tripathi, *J. Energy Storage* **2019**, *21*, 801.

[47] C. Prehal, H. Fitzek, G. Kothleitner, V. Presser, B. Gollas, S. A. Freunberger, Q. Abbas, *Nat. Commun.* **2020**, *11*, 4838.

[48] D. Zhao, C. Chen, Q. Zhang, W. Chen, S. Liu, Q. Wang, Y. Liu, J. Li, H. Yu, *Adv. Energy Mater.* **2017**, *7*, 1700739.

[49] A. González, E. Goikolea, J. A. Barrena, R. Mysyk, *Renewable Sustainable Energy Rev.* **2016**, *58*, 1189.

[50] W. Raza, F. Ali, N. Raza, Y. Luo, K. H. Kim, J. Yang, S. Kumar, A. Mehmood, E. E. Kwon, *Nano Energy* **2018**, *52*, 441.

[51] C. Siu, K. Iniewski, *IoT and Low-Power Wireless*, CRC Press, Boca Raton, FL, **2018**.

[52] L. Portilla, J. Zhao, Y. Wang, L. Sun, F. Li, M. Robin, M. Wei, Z. Cui, L. G. Occhipinti, T. D. Anthopoulos, V. Pecunia, *ACS Nano* **2020**, *14*, 14036.

[53] T. Jang, M. Choi, M. Shi, I. Lee, D. Sylvester, D. Blaauw, *2016 IEEE Int. Conf. RFID*, IEEE, Piscataway **2016**, pp. 1–4.

[54] S. Oh, M. Cho, X. Wu, Y. Kim, L.-X. Chuo, W. Lim, P. Pannuto, S. Bang, K. Yang, H.-S. Kim, D. Sylvester, D. Blaauw, in *2019 Des. Autom. Test Eur. Conf. Exhib.*, IEEE, Piscataway **2019**, pp. 686–691.

[55] O. Georgiou, K. Mimis, D. Halls, W. H. Thompson, D. Gibbins, *IEEE Access* **2016**, *4*, 3732.

[56] M. T. Todaro, F. Guido, L. Algieri, V. M. Mastronardi, D. Desmaele, G. Epifani, M. De Vittorio, *IEEE Trans. Nanotechnol.* **2018**, *17*, 220.

[57] H. Michaels, I. Benesperi, M. Freitag, *Chem. Sci.* **2021**, *12*, 5002.

[58] L. Smith, T. Ibn-Mohammed, L. Koh, I. M. Reaney, *J. Am. Ceram. Soc.* **2019**, *102*, 7037.

[59] H. Ambrose, A. Kendall, *J. Ind. Ecol.* **2020**, *24*, 90.

[60] H. H. R. Sherazi, M. A. Imran, G. Boggia, L. A. Grieco, *IEEE Commun. Lett.* **2018**, *22*, 2358.

[61] W. S. Wang, T. O'Donnell, N. Wang, M. Hayes, B. O'Flynn, C. O'Mathuna, *ACM J. Emerg. Technol. Comput. Syst.* **2010**, *6*, 1.

[62] V. Pecunia, M. Fattori, S. Abdinia, H. Sirringhaus, E. Cantatore, *Organic and Amorphous-Metal-Oxide Flexible Analogue Electronics*, Cambridge University Press, Cambridge, UK **2018**.

[63] M. Alioto (Ed.), *Enabling the Internet of Things*, Springer International Publishing, Cham **2017**.

[64] P. Kamalinejad, C. Mahapatra, Z. Sheng, S. Mirabbasi, V. C. M. Leung, Y. L. Guan, *IEEE Commun. Mag.* **2015**, *53*, 102.

[65] M. Shirvanimoghaddam, K. Shirvanimoghaddam, M. M. Abolhasani, M. Farhangi, V. Zahiri Barsari, H. Liu, M. Dohler, M. Naebe, *IEEE Access* **2019**, *7*, 94533.

[66] J. Henkel, S. Pagani, H. Amrouch, L. Bauer, F. Samie, *Design, Automation & Test in Europe Conference & Exhibition*, IEEE, Piscataway **2017**, pp. 954–959.

[67] R. J. M. Vullers, R. van Schaijk, I. Doms, C. Van Hoof, R. Mertens, *Solid-State Electron.* **2009**, *53*, 684.

[68] Silicon Laboratories, Inc. Implementing Energy Harvesting in Embedded System Designs, https://www.silabs.com/documents/public/white-papers/implementing-energy-harvesting-in-embedded-system-designs.pdf (accessed: February 2021).

[69] D. M. Rowe (Ed.), *Thermoelectrics and Its Energy Harvesting, 2-Volume Set*, CRC Press, Boca Raton, FL **2018**.

[70] M. Freunek Müller (Ed.), *Indoor Photovoltaics*, Wiley, Hoboken, NJ **2020**.

[71] F. Sangare, Z. Han, *Wireless Information and Power Transfer: A New Paradigm for Green Communications*, Springer International Publishing, Cham **2018**, pp. 189–239.

[72] C. R. Bowen, V. Y. Topolov, H. A. Kim, *Modern Piezoelectric Energy-Harvesting Materials*, Springer International Publishing, Cham **2016**.

[73] Z. L. Wang, L. Lin, J. Chen, S. Niu, Y. Zi, *TriboelectricNanogenerators*, Springer International Publishing, Cham **2016**.

[74] D. M. Rowe (Ed.), *Thermoelectrics Handbook*, CRC Press, Boca Raton, FL **2018**.

[75] M. Haras, T. Skotnicki, *Nano Energy* **2018**, *54*, 461.

[76] V. Leonov, *IEEE Sens. J.* **2013**, *13*, 2284.

[77] V. Leonov, R. J. M. Vullers, *J. Renewable Sustainable Energy* **2009**, *1*, 062701.

[78] R. Freer, A. V. Powell, *J. Mater. Chem. C* **2020**, *8*, 441.

[79] Y. Du, J. Xu, B. Paul, P. Eklund, *Appl. Mater. Today* **2018**, *12*, 366.

[80] L. Yang, Z.-G. Chen, M. S. Dargusch, J. Zou, *Adv. Energy Mater.* **2018**, *8*, 1701797.

[81] M. S. Dresselhaus, G. Chen, M. Y. Tang, R. G. Yang, H. Lee, D. Z. Wang, Z. F. Ren, J.-P. Fleurial, P. Gogna, *Adv. Mater.* **2007**, *19*, 1043.

[82] J.-H. Bahk, H. Fang, K. Yazawa, A. Shakouri, *J. Mater. Chem. C* **2015**, *3*, 10362.

[83] R. K. Iyer, S. Pilla, *Sci. Total Environ.* **2021**, *752*, 141674.

[84] R. Amatya, R. J. Ram, *J. Electron. Mater.* **2012**, *41*, 1011.

[85] R. Vizel, T. Bargig, O. Beeri, Y. Gelbstein, *J. Electron. Mater.* **2016**, *45*, 1296.

[86] S. LeBlanc, *Sustainable Mater. Technol.* **2014**, *1–2*, 26.

**ADVANCED
SCIENCE NEWS**

www.advancedsciencenews.com

**ADVANCED
ENERGY
MATERIALS**

www.advenergymat.de

[87] M. S. Hossain, T. Li, Y. Yu, J. Yong, J.-H. Bahk, E. Skafidas, *RSC Adv.* **2020**, *10*, 8421.

[88] Q. Zhang, Y. Sun, W. Xu, D. Zhu, *Adv. Mater.* **2014**, *26*, 6829.

[89] Z. Fan, Y. Zhang, L. Pan, J. Ouyang, Q. Zhang, *Renewable Sustainable Energy Rev.* **2021**, *137*, 110448.

[90] G.-H. Kim, L. Shao, K. Zhang, K. P. Pipe, *Nat. Mater.* **2013**, *12*, 719.

[91] S. Priya, H.-C. Song, Y. Zhou, R. Varghese, A. Chopra, S.-G. Kim, I. Kanno, L. Wu, D. S. Ha, J. Ryu, R. G. Polcawich, *Energy Harvesting and Systems*, Walter de Gruyter Inc., Boston **2019**

[92] Z. Wen, Y. Yang, N. Sun, G. Li, Y. Liu, C. Chen, J. Shi, L. Xie, H. Jiang, D. Bao, Q. Zhuo, X. Sun, *Adv. Funct. Mater.* **2018**, *28*, 1803684.

[93] Z. L. Wang, J. Chen, L. Lin, *Energy Environ. Sci.* **2015**, *8*, 2250.

[94] H. Sun, Y. Guo, M. He, Z. Zhong, *IEEE Antennas Wirel. Propag. Lett.* **2013**, *12*, 918.

[95] P. Momenroodaki, R. D. Fernandes, Z. Popovic, *2016 10th Eur. Conf. on Antennas and Propagation*, IEEE, Piscataway **2016**, pp. 1–4.

[96] R. Vullers, R. Schaijk, H. Visser, J. Penders, C. Hoof, *IEEE Solid-State Circuits Mag.* **2010**, *2*, 29.

[97] Z. Cao, E. Koukharenko, R. N. Torah, J. Tudor, S. P. Beeby, *J. Phys.: Conf. Ser.* **2014**, *557*, 012016.

[98] Z. Zhang, J. Qiu, S. Wang, *Manuf. Lett.* **2016**, *8*, 6.

[99] M. Tomita, S. Oba, Y. Himeda, R. Yamato, K. Shima, T. Kumada, M. Xu, H. Takezawa, K. Mesaki, K. Tsuda, S. Hashimoto, T. Zhan, H. Zhang, Y. Kamakura, Y. Suzuki, H. Inokawa, H. Ikeda, T. Matsukawa, T. Matsuki, T. Watanabe, *2018 IEEE Symp. VLSI Technol.*, IEEE, Piscataway **2018**, pp. 93–94.

[100] Z. Li, H. Sun, C.-L. Hsiao, Y. Yao, Y. Xiao, M. Shahi, Y. Jin, A. Cruce, X. Liu, Y. Jiang, W. Meng, F. Qin, T. Ederth, S. Fabiano, W. M. Chen, X. Lu, J. Birch, J. W. Brill, Y. Zhou, X. Crispin, F. Zhang, *Adv. Electron. Mater.* **2018**, *4*, 1700496.

[101] H. Bottner, J. Nurnus, A. Gavrikov, G. Kuhner, M. Jagle, C. Kunzel, D. Eberhard, G. Plescher, A. Schubert, K.-H. Schlereth, *J. Microelectromech. Syst.* **2004**, *13*, 414.

[102] A. Ahmed, I. Hassan, A. S. Helal, V. Sencadas, A. Radhi, C. K. Jeong, M. F. El-Kady, *iScience* **2020**, *23*, 101286.

[103] X. He, Q. Wen, Z. Lu, Z. Shang, Z. Wen, *Appl. Energy* **2018**, *228*, 881.

[104] T. Hehn, Y. Manoli, *CMOS Circuits for Piezoelectric Energy Harvesters*, Springer, Netherlands, Dordrecht **2015**.

[105] Y. Liu, H. Khanbareh, M. A. Halim, A. Feeney, X. Zhang, H. Heidari, R. Ghannam, *Nano Select* **2021**, *1*, https://doi.org/10.1002/nano.202000242.

[106] T. Ibn-Mohammed, I. M. Reaney, S. C. L. Koh, A. Acquaye, D. C. Sinclair, C. A. Randall, F. H. Abubakar, L. Smith, G. Schileo, L. Ozawa-Meida, *J. Eur. Ceram. Soc.* **2018**, *38*, 4922.

[107] F. Cucchiella, I. D'Adamo, S. C. Lenny Koh, P. Rosa, *Renewable Sustainable Energy Rev.* **2015**, *51*, 263.

[108] D. Fasquelle, M. Mascot, N. Sama, D. Remiens, J.-C. Carru, *Sens. Actuators, A.* **2015**, *229*, 30.

[109] A. J. Bell, O. Deubzer, *MRS Bull.* **2018**, *43*, 581.

[110] Y. Saito, H. Takao, T. Tani, T. Nonoyama, K. Takatori, T. Homma, T. Nagaya, M. Nakamura, *Nature* **2004**, *432*, 84.

[111] T. Ibn-Mohammed, S. C. L. Koh, I. M. Reaney, A. Acquaye, D. Wang, S. Taylor, A. Genovese, *Energy Environ. Sci.* **2016**, *9*, 3495.

[112] T. Ibn-Mohammed, S. C. L. Koh, I. M. Reaney, D. C. Sinclair, K. B. Mustapha, A. Acquaye, D. Wang, *MRS Commun.* **2017**, *7*, 1.

[113] M. Safaei, H. A. Sodano, S. R. Anton, *Smart Mater. Struct.* **2019**, *28*, 113001.

[114] N. Sezer, M. Koç, *Nano Energy* **2021**, *80*, 105567.

[115] Y. S. Choi, S. K. Kim, M. Smith, F. Williams, M. E. Vickers, J. A. Elliott, S. Kar-Narayan, *Sci. Adv.* **2020**, *6*, eaay5065.

[116] G. Laroche, Y. Marois, R. Guidoin, M. W. King, L. Martin, T. How, Y. Douville, *J. Biomed. Mater. Res.* **1995**, *29*, 1525.

[117] Z. L. Wang, A. C. Wang, *Mater. Today* **2019**, *30*, 34.

[118] Y. Zhou, W. Deng, J. Xu, J. Chen, *Cell Rep. Phys. Sci.* **2020**, *1*, 100142.

[119] Z. L. Wang, *Adv. Energy Mater.* **2020**, *10*, 2000137.

[120] Z. Liu, H. Li, B. Shi, Y. Fan, Z. L. Wang, Z. Li, *Adv. Funct. Mater.* **2019**, *29*, 1808820.

[121] J. Chen, Z. L. Wang, *Joule* **2017**, *1*, 480.

[122] D. W. Kim, J. H. Lee, J. K. Kim, U. Jeong, *NPG Asia Mater.* **2020**, *12*, 6.

[123] L. Dhakar, S. Gudla, X. Shan, Z. Wang, F. E. H. Tay, C.-H. Heng, C. Lee, *Sci. Rep.* **2016**, *6*, 22253.

[124] A. Ahmed, I. Hassan, T. Ibn-Mohammed, H. Mostafa, I. M. Reaney, L. S. C. Koh, J. Zu, Z. L. Wang, *Energy Environ. Sci.* **2017**, *10*, 653.

[125] V. Slabov, S. Kopyl, M. P. Soares dos Santos, A. L. Kholkin, *Nano-Micro Lett.* **2020**, *12*, 42.

[126] A. P. Sample, A. N. Parks, S. Southwood, J. R. Smith, in *Wirelessly Powered Sens. Networks Comput. RFID* (Ed: J. R. Smith), Springer New York, New York, NY **2013**, pp. 223–234.

[127] H. T. Friis, *Proc. IRE Waves Electrons* **1946**, *34*, 254.

[128] T. K. Sarkar, Z. Ji, K. Kim, A. Medouri, M. Salazar-Palma, *IEEE Antennas Propag. Mag.* **2003**, *45*, 51.

[129] S. Kim, M. M. Tentzeris, A. Georgiadis, *Sensors* **2019**, *19*, 728.

[130] S. Kim, R. Vyas, J. Bito, K. Niotaki, A. Collado, A. Georgiadis, M. M. Tentzeris, *Proc. IEEE* **2014**, *102*, 1649.

[131] F. Meng, J. Huang, *AIP Adv.* **2018**, *8*, 085118.

[132] V. Palazzi, J. Hester, J. Bito, F. Alimenti, C. Kalialakis, A. Collado, P. Mezzanotte, A. Georgiadis, L. Roselli, M. M. Tentzeris, *IEEE Trans. Microwave Theory Tech.* **2018**, *66*, 366.

[133] C. R. Valenta, G. D. Durgin, *IEEE Microwave Mag.* **2014**, *15*, 108.

[134] S. B. Boyd, *Life-Cycle Assessment of Semiconductors*, Springer New York, NY **2012**.

[135] D. G. Georgiadou, J. Semple, A. A. Sagade, H. Forstén, P. Rantakari, Y.-H. Lin, F. Alkhalil, A. Seitkhan, K. Loganathan, H. Faber, T. D. Anthopoulos, *Nat. Electron.* **2020**, *3*, 718.

[136] J. Semple, D. G. Georgiadou, G. Wyatt-Moon, G. Gelinck, T. D. Anthopoulos, *Semicond. Sci. Technol.* **2017**, *32*, 123002.

[137] D. L. Dilaura, K. W. Houser, R. G. Mistrick, G. R. Steffy (Eds.), *The Lighting Handbook: Reference and Application*, Illuminating Engineering Society Of North America, NY **2011**.

[138] Y. Peng, T. N. Huq, J. Mei, L. Portilla, R. A. Jagt, L. G. Occhipinti, J. L. MacManus-Driscoll, R. L. Z. Hoye, V. Pecunia, *Adv. Energy Mater.* **2021**, *11*, 2002761.

[139] A. S. Teran, J. Wong, W. Lim, G. Kim, Y. Lee, D. Blaauw, J. D. Phillips, *IEEE Trans. Electron Devices* **2015**, *62*, 2170.

[140] I. M. Peters, T. Buonassisi, *Joule* **2018**, 1160.

[141] K. O. Hara, N. Usami, *J. Appl. Phys.* **2013**, *114*, 153101.

[142] V. Pecunia, J. Zhao, C. Kim, B. R. Tuttle, J. Mei, F. Li, Y. Peng, T. N. Huq, R. L. Z. Hoye, N. D. Kelly, S. E. Dutton, K. Xia, J. L. MacManus-Driscoll, H. Sirringhaus, *Adv. Energy Mater.* **2021**, 2003968, https://doi.org/10.1002/aenm.202003968.

[143] P. Calado, D. Burkitt, J. Yao, J. Troughton, T. M. Watson, M. J. Carnie, A. M. Telford, B. C. O'Regan, J. Nelson, P. R. F. Barnes, *Phys. Rev. Appl.* **2019**, *11*, 044005.

[144] W. Tress, M. Yavari, K. Domanski, P. Yadav, B. Niesen, J. P. Correa Baena, A. Hagfeldt, M. Graetzel, *Energy Environ. Sci.* **2018**, *11*, 151.

[145] G. E. Bunea, K. E. Wilson, Y. Meydbray, M. P. Campbell, D. M. De Ceuster, *2006 IEEE 4th World Conf. on Photovoltaic Energy Conf.*, IEEE, Piscataway **2006**, pp. 1312–1314.

[146] *Photovoltaics Report*, Fraunhofer Institute for Solar Energy Systems, **2019**.

[147] N. H. Reich, W. G. J. H. M. van Sark, W. C. Turkenburg, *Renewable Energy* **2011**, *36*, 642.

[148] F. De Rossi, T. Pontecorvo, T. M. Brown, *Appl. Energy* **2015**, *156*, 413.

[149] M. Freunek Müller, M. Freunek, L. M. Reindl, *IEEE J. Photovoltaic* **2013**, *3*, 59.

[150] D. T. Cotfas, P. A. Cotfas, *Int. J. Photoenergy* **2019**, *2019*, 1905041.

**ADVANCED
SCIENCE NEWS**

www.advancedsciencenews.com

**ADVANCED
ENERGY
MATERIALS**

www.advenergymat.de

[151] G. Apostolou, A. Reinders, M. Verwaal, *Energy Sci. Eng.* **2016**, *4*, 69.

[152] M. F. Müller (Ed.), *Photovoltaic Modeling Handbook*, John Wiley & Sons, Inc., Hoboken, NJ **2018**.

[153] M. Li, F. Igbari, Z. Wang, L. Liao, *Adv. Energy Mater.* **2020**, *10*, 2000641.

[154] I. Mathews, P. J. King, F. Stafford, R. Frizzell, *IEEE J. Photovoltaic* **2016**, *6*, 230.

[155] M. Freitag, J. Teuscher, Y. Saygili, X. Zhang, F. Giordano, P. Liska, J. Hua, S. M. Zakeeruddin, J. E. Moser, M. Grätzel, A. Hagfeldt, *Nat. Photonics* **2017**, *11*, 372.

[156] H. K. H. Lee, J. Wu, J. Barbé, S. M. Jain, S. Wood, E. M. Speller, Z. Li, F. A. Castro, J. R. Durrant, W. C. Tsoi, *J. Mater. Chem. A* **2018**, *6*, 5618.

[157] Z. Ding, R. Zhao, Y. Yu, J. Liu, *J. Mater. Chem. A* **2019**, *7*, 26533.

[158] M. Stuckelberger, R. Biron, N. Wyrsch, F. J. Haug, C. Ballif, *Renewable Sustainable Energy Rev.* **2017**, *76*, 1497.

[159] H. K. Charles, A. P. Ariotedjo, *Sol. Energy* **1980**, *24*, 329.

[160] R. A. Street, *Hydrogenated Amorphous Silicon*, Cambridge University Press, Cambridge, UK **1991**.

[161] D. E. Carlson, *IEEE Trans. Electron Devices* **1989**, *36*, 2775.

[162] F. Bella, C. Gerbaldi, C. Barolo, M. Grätzel, *Chem. Soc. Rev.* **2015**, *44*, 3431.

[163] S. Zhang, X. Yang, C. Qin, Y. Numata, L. Han, *J. Mater. Chem. A* **2014**, *2*, 5167.

[164] R. Khajavian, M. Mirzaei, H. Alizadeh, *Dalton Trans.* **2020**, *49*, 13936.

[165] R. Steim, F. R. Kogler, C. J. Brabec, *J. Mater. Chem.* **2010**, *20*, 2499.

[166] H. Zhang, Y. Li, X. Zhang, Y. Zhang, H. Zhou, *Mater. Chem. Front.* **2020**, *4*, 2863.

[167] E. L. Ratcliff, B. Zacher, N. R. Armstrong, *J. Phys. Chem. Lett.* **2011**, *2*, 1337.

[168] H. Xu, F. Yuan, D. Zhou, X. Liao, L. Chen, Y. Chen, *J. Mater. Chem. A* **2020**, *8*, 11478.

[169] S. P. Dunfield, L. Bliss, F. Zhang, J. M. Luther, K. Zhu, M. F. A. M. van Hest, M. O. Reese, J. J. Berry, *Adv. Energy Mater.* **2020**, *10*, 1904054.

[170] C. A. R. Perini, T. A. S. Doherty, S. D. Stranks, J.-P. Correa-Baena, R. L. Z. Hoye, *Joule* **2021**, *5*, 1024.

[171] S. Y. Kim, S. J. Cho, S. E. Byeon, X. He, H. J. Yoon, *Adv. Energy Mater.* **2020**, *10*, 2002606.

[172] H. Lu, A. Krishna, S. M. Zakeeruddin, M. Grätzel, A. Hagfeldt, *iScience* **2020**, *23*, 101359.

[173] X. Zhang, Y. Xu, F. Giordano, M. Schreier, N. Pellet, Y. Hu, C. Yi, N. Robertson, J. Hua, S. M. Zakeeruddin, H. Tian, M. Grätzel, *J. Am. Chem. Soc.* **2016**, *138*, 10742.

[174] D. P. Hagberg, T. Marinado, K. M. Karlsson, K. Nonomura, P. Qin, G. Boschloo, T. Brinck, A. Hagfeldt, L. Sun, *J. Org. Chem.* **2007**, *72*, 9550.

[175] K. Fukutani, M. Kanbe, W. Futako, B. Kaplan, T. Kamiya, C. Fortmann, I. Shimizu, *J. Non-Cryst. Solids* **1998**, *227–230*, 63.

[176] R. E. Hollingsworth, P. K. Bhat, A. Madan, *J. Non-Cryst. Solids* **1987**, *97–98*, 309.

[177] M. Otsuka, Y. Kurokawa, Y. Ding, F. B. Juangsa, S. Shibata, T. Kato, T. Nozaki, *RSC Adv.* **2020**, *10*, 12611.

[178] P. K. Nayak, S. Mahesh, H. J. Snaith, D. Cahen, *Nat. Rev. Mater.* **2019**, *4*, 269.

[179] D. L. Staebler, C. R. Wronski, *J. Appl. Phys.* **1980**, *51*, 3262.

[180] M. A. Kreiger, D. R. Shonnard, J. M. Pearce, *Resour., Conserv. Recycl.* **2013**, *70*, 44.

[181] M.-H. Kao, C.-H. Shen, P. Yu, W.-H. Huang, Y.-L. Chueh, J.-M. Shieh, *Sci. Rep.* **2017**, *7*, 12706.

[182] D. J. You, S.-H. Kim, H. Lee, J.-W. Chung, S.-T. Hwang, Y. H. Heo, S. Lee, H.-M. Lee, *Prog. Photovoltaics* **2015**, *23*, 973.

[183] R. Crandall, W. Luft, *Prog. Photovoltaics* **1995**, *3*, 315.

[184] Global Markets, Technologies and Devices for Energy Harvesting: EGY097C, https://www.bccresearch.com/market-research/energy-and-resources/global-markets-technologies-and-devices-for-energy-harvesting.html (accessed: February 2021).

[185] R. Terasa, A. Kottwitz, J. Kuske, U. Stephan, J. W. Bartha, *Record of the Thirty-first IEEE Photovoltaic Specialists Conf.*, IEEE, Piscataway, **2005**, pp. 1528–1531.

[186] T. K. Subramanyam, S. P. Kumar, P. Goutham, R. Suresh, K. N. Subramanya, *Mater. Today: Proc.* **2018**, *5*, 21061.

[187] T. Ibn-Mohammed, S. C. L. Koh, I. M. Reaney, A. Acquaye, G. Schileo, K. B. Mustapha, R. Greenough, *Renewable Sustainable Energy Rev.* **2017**, *80*, 1321.

[188] M. L. Parisi, S. Maranghi, R. Basosi, *Renewable Sustainable Energy Rev.* **2014**, *39*, 124.

[189] S. Lizin, S. Van Passel, E. De Schepper, W. Maes, L. Lutsen, J. Manca, D. Vanderzande, *Energy Environ. Sci.* **2013**, *6*, 3136.

[190] U.S. Geological Survey, Mineral Commodity Summaries, **2020**.

[191] J. H. Wong, M. Royapoor, C. W. Chan, *Renewable Sustainable Energy Rev.* **2016**, *58*, 608.

[192] Health and Safety Executive, Control of Lead at Work (Third Edition) https://www.hse.gov.uk/pubns/priced/l132.pdf (accessed: February 2021).

[193] Health and Safety Executive, EH40 /2005 Workplace Exposure Limits Limits for Use with the Control of Substances (Fourth Edition 2020), https://www.hse.gov.uk/pubns/books/eh40.htm (accessed: February 2021).

[194] R. Vidal, J.-A. Alberola-Borràs, G.-M. Joaquín-Luis, S. N. Habisreutinger, D. T. Moore, T. H. Schloemer, I. Mora-Seró, J. J. Berry, J. M. Luther, *Nat. Sustain.* **2020**, *4*, 277.

[195] B. O'Regan, M. Grätzel, *Nature* **1991**, *353*, 737.

[196] M. Grätzel, *Nature* **2001**, *414*, 338.

[197] K. Takagi, S. Magaino, H. Saito, T. Aoki, D. Aoki, *J. Photochem. Photobiol., C* **2013**, *14*, 1.

[198] N. Mariotti, M. Bonomo, L. Fagiolari, N. Barbero, C. Gerbaldi, F. Bella, C. Barolo, *Green Chem.* **2020**, *22*, 7168.

[199] *Dye Sensitized Solar Cell Market Size, Share & Trends Analysis Report By Application (Portable Charging, BIPV/BAPV, Embedded Electronics, Outdoor Advertising, Automotive (AIPV)), And Segment Forecasts, 2020–2027*, **2020**.

[200] S. Mozaffari, M. R. Nateghi, M. B. Zarandi, *Renewable Sustainable Energy Rev.* **2017**, *71*, 675.

[201] H. Iftikhar, G. G. Sonai, S. G. Hashmi, A. F. Nogueira, P. D. Lund, *Materials* **2019**, *12*, 1998.

[202] R. Harikisun, H. Desilvestro, *Sol. Energy* **2011**, *85*, 1179.

[203] J. B. Baxter, *J. Vac. Sci. Technol., A* **2012**, *30*, 020801.

[204] Y. Cao, Y. Saygili, A. Ummadisingu, J. Teuscher, J. Luo, N. Pellet, F. Giordano, S. M. Zakeeruddin, J. E. Moser, M. Freitag, A. Hagfeldt, M. Grätzel, *Nat. Commun.* **2017**, *8*, 15390.

[205] W. Zhang, Y. Wu, H. W. Bahng, Y. Cao, C. Yi, Y. Saygili, J. Luo, Y. Liu, L. Kavan, J. E. Moser, A. Hagfeldt, H. Tian, S. M. Zakeeruddin, W. H. Zhu, M. Grätzel, *Energy Environ. Sci.* **2018**, *11*, 1779.

[206] A. Fakharuddin, R. Jose, T. M. Brown, F. Fabregat-Santiago, J. Bisquert, *Energy Environ. Sci.* **2014**, *7*, 3952.

[207] S. Datta, A. Dey, N. R. Singha, S. Roy, *Mater. Renewable Sustainable Energy* **2020**, *9*, 25.

[208] N. Mariotti, M. Bonomo, C. Barolo, in *Reliability and Ecological Aspects of Photovoltaic Module* (Ed: A. Gok), IntechOpen **2020**, Ch. 8, https://doi.org/10.5772/intechopen.88327.

[209] M. L. Parisi, A. Dessì, L. Zani, S. Maranghi, S. Mohammadpourasl, M. Calamante, A. Mordini, R. Basosi, G. Reginato, A. Sinicropi, *Front. Chem.* **2020**, *8*, 214.

[210] M. L. Parisi, S. Maranghi, L. Vesce, A. Sinicropi, A. Di Carlo, R. Basosi, *Renewable Sustainable Energy Rev.* **2020**, *121*, 109703.

[211] A. Köhler, H. Bässler, *Electronic Processes in Organic Semiconductors*, Wiley-VCH Verlag GmbH & Co. KGaA, Weinheim, Germany **2015**, pp. 307–388.

**ADVANCED
SCIENCE NEWS**

www.advancedsciencenews.com

**ADVANCED
ENERGY
MATERIALS**

www.advenergymat.de

[212] V. Pecunia, *Organic Narrowband Photodetectors: Materials Devices and Applications*, IOP Publishing, Bristol, UK **2019**.

[213] J. Hou, O. Inganäs, R. H. Friend, F. Gao, *Nat. Mater.* **2018**, *17*, 119.

[214] C. Yan, S. Barlow, Z. Wang, H. Yan, A. K.-Y. Jen, S. R. Marder, X. Zhan, *Nat. Rev. Mater.* **2018**, *3*, 18003.

[215] E. A. Chandross, *Science* **2011**, *333*, 35.

[216] C. B. Nielsen, S. Holliday, H.-Y. Chen, S. J. Cryer, I. McCulloch, *Acc. Chem. Res.* **2015**, *48*, 2803.

[217] M. Corazza, F. C. Krebs, S. A. Gevorgyan, *Sol. Energy Mater. Sol. Cells* **2015**, *143*, 467.

[218] X. Du, T. Heumueller, W. Gruber, A. Classen, T. Unruh, N. Li, C. J. Brabec, *Joule* **2019**, *3*, 215.

[219] F. Lin, K. Jiang, W. Kaminsky, Z. Zhu, A. K.-Y. Jen, *J. Am. Chem. Soc.* **2020**, *142*, 15246.

[220] Y. Cui, Y. Wang, J. Bergqvist, H. Yao, Y. Xu, B. Gao, C. Yang, S. Zhang, O. Inganäs, F. Gao, J. Hou, *Nat. Energy* **2019**, *4*, 768.

[221] A. Anctil, C. W. Babbitt, R. P. Raffaelle, B. J. Landi, *Environ. Sci. Technol.* **2011**, *45*, 2353.

[222] R. García-Valverde, J. A. Cherni, A. Urbina, *Prog. Photovoltaics* **2010**, *18*, 535.

[223] A. Anctil, C. W. Babbitt, R. P. Raffaelle, B. J. Landi, *Prog. Photovoltaics* **2013**, *21*, 1541.

[224] F. C. Krebs, *Sol. Energy Mater. Sol. Cells* **2009**, *93*, 394.

[225] Y.-S. Zimmermann, A. Schäffer, C. Hugi, K. Fent, P. F.-X. Corvini, M. Lenz, *Environ. Int.* **2012**, *49*, 128.

[226] J. Xue, R. Wang, Y. Yang, *Nat. Rev. Mater.* **2020**, *5*, 809.

[227] K. X. Steirer, P. Schulz, G. Teeter, V. Stevanovic, M. Yang, K. Zhu, J. J. Berry, *ACS Energy Lett.* **2016**, *1*, 360.

[228] M. D. Smith, B. A. Connor, H. I. Karunadasa, *Chem. Rev.* **2019**, *119*, 3104.

[229] A. Kojima, K. Teshima, Y. Shirai, T. Miyasaka, *J. Am. Chem. Soc.* **2009**, *131*, 6050.

[230] NREL, **2020**.

[231] J. Jeong, M. Kim, J. Seo, H. Lu, P. Ahlawat, A. Mishra, Y. Yang, M. A. Hope, F. T. Eickemeyer, M. Kim, Y. J. Yoon, I. W. Choi, B. P. Darwich, S. J. Choi, Y. Jo, J. H. Lee, B. Walker, S. M. Zakeeruddin, L. Emsley, U. Rothlisberger, A. Hagfeldt, D. S. Kim, M. Grätzel, J. Y. Kim, *Nature* **2021**, *592*, 381.

[232] J. J. Yoo, G. Seo, M. R. Chua, T. G. Park, Y. Lu, F. Rotermund, Y. Kim, C. S. Moon, N. J. Jeon, V. Bulović, S. S. Shin, M. G. Bawendi, *Nature* **2021**, *590*, 587.

[233] A. Polman, M. Knight, E. C. Garnett, B. Ehrler, W. C. Sinke, *Science* **2016**, *352*, aad4424.

[234] R. Cheng, C. C. Chung, H. Zhang, F. Liu, W. T. Wang, Z. Zhou, S. Wang, A. B. Djurišić, S. P. Feng, *Adv. Energy Mater.* **2019**, *9*, 1901980.

[235] A. Senocrate, G. Y. Kim, M. Grätzel, J. Maier, *ACS Energy Lett.* **2019**, *4*, 2859.

[236] A. F. Palmstrom, J. A. Raiford, R. Prasanna, K. A. Bush, M. Sponseller, R. Cheacharoen, M. C. Minichetti, D. S. Bergsman, T. Leijtens, H. P. Wang, V. Bulović, M. D. McGehee, S. F. Bent, *Adv. Energy Mater.* **2018**, *8*, 1800591.

[237] J. Zhao, K. O. Brinkmann, T. Hu, N. Pourdavoud, T. Becker, T. Gahlmann, R. Heiderhoff, A. Polywka, P. Görrn, Y. Chen, B. Cheng, T. Riedl, *Adv. Energy Mater.* **2017**, *7*, 1602599.

[238] R. D. Raninga, R. A. Jagt, S. Béchu, T. N. Huq, W. Li, M. Nikolka, Y.-H. Lin, M. Sun, Z. Li, W. Li, M. Bouttemy, M. Frégnaux, H. J. Snaith, P. Schulz, J. L. MacManus-Driscoll, R. L. Z. Hoye, *Nano Energy* **2020**, *75*, 104946.

[239] K. A. Bush, C. D. Bailie, Y. Chen, T. Leijtens, A. R. Bowring, F. Moghadam, M. D. McGehee, *Adv. Mater.* **2016**, *28*, 3937.

[240] K. A. Bush, A. F. Palmstrom, Z. J. Yu, M. Boccard, R. Cheacharoen, J. P. Mailoa, D. P. McMeekin, R. L. Z. Hoye, C. D. Bailie, T. Leijtens, I. M. Peters, M. C. Minichetti, N. Rolston, R. Prasanna, S. Sofia, D. Harwood, W. Ma, F. Moghadam, H. J. Snaith, T. Buonassisi, Z. C. Holman, S. F. Bent, M. D. McGehee, *Nat. Energy* **2017**, *2*, 17009.

[241] J. J. Yoo, S. Wieghold, M. C. Sponseller, M. R. Chua, S. N. Bertram, N. T. P. Hartono, J. S. Tresback, E. C. Hansen, J. P. Correa-Baena, V. Bulović, T. Buonassisi, S. S. Shin, M. G. Bawendi, *Energy Environ. Sci.* **2019**, *12*, 2192.

[242] I. C. Smith, E. T. Hoke, D. Solis-Ibarra, M. D. McGehee, H. I. Karunadasa, *Angew. Chem., Int. Ed.* **2014**, *53*, 11232; *Angew. Chem.* **2014**, *126*, 11414.

[243] G. Grancini, C. Roldán-Carmona, I. Zimmermann, E. Mosconi, X. Lee, D. Martineau, S. Narbey, F. Oswald, F. De Angelis, M. Graetzel, M. K. Nazeeruddin, *Nat. Commun.* **2017**, *8*, 15684.

[244] C. C. Boyd, R. C. Shallcross, T. Moot, R. Kerner, L. Bertoluzzi, A. Onno, S. Kavadiya, C. Chosy, E. J. Wolf, J. Werner, J. A. Raiford, C. de Paula, A. F. Palmstrom, Z. J. Yu, J. J. Berry, S. F. Bent, Z. C. Holman, J. M. Luther, E. L. Ratcliff, N. R. Armstrong, M. D. McGehee, *Joule* **2020**, *4*, 1759.

[245] A. Al-Ashouri, E. Köhnen, B. Li, A. Magomedov, H. Hempel, P. Caprioglio, J. A. Márquez, A. Belen Maorales Vilches, E. Kasparavicius, J. A. Smith, N. Phung, D. Menzel, M. Grischek, L. Kegelmann, C. Skroblin, C. Gollwitzer, T. Malinauskas, M. Jost, G. Matic, B. Rech, R. Schlatmann, M. Topic, L. Korte, A. Abate, B. Stannowski, D. Neher, M. Stolterfoht, T. Unold, V. Getautis, S. Albrecht, *Science* **2020**, *370*, 1300.

[246] S. S. Shin, E. J. Yeom, W. S. Yang, S. Hur, M. G. Kim, J. Im, J. Seo, J. H. Noh, S. Il Seok, *Science* **2017**, *356*, 167.

[247] M. Cai, Y. Wu, H. Chen, X. Yang, Y. Qiang, L. Han, *Adv. Sci.* **2017**, *4*, 1600269.

[248] Z. Li, Y. Zhao, X. Wang, Y. Sun, Z. Zhao, Y. Li, H. Zhou, Q. Chen, *Joule* **2018**, *2*, 1559.

[249] Y. Deng, C. H. van Brackle, X. Dai, J. Zhao, B. Chen, J. Huang, *Sci. Adv.* **2019**, *5*, eaax7537.

[250] Z. Li, P. Li, G. Chen, Y. Cheng, X. Pi, X. Yu, D. Yang, L. Han, Y. Zhang, Y. Song, *ACS Appl. Mater. Interfaces* **2020**, *12*, 39082.

[251] N. Rolston, W. J. Scheideler, A. C. Flick, J. P. Chen, H. Elmaraghi, A. Sleugh, O. Zhao, M. Woodhouse, R. H. Dauskardt, *Joule* **2020**, *4*, 2675.

[252] C. Momblona, L. Gil-Escrig, E. Bandiello, E. M. Hutter, M. Sessolo, K. Lederer, J. Blochwitz-Nimoth, H. J. Bolink, *Energy Environ. Sci.* **2016**, *9*, 3456.

[253] L. Qiu, S. He, Y. Jiang, D.-Y. Son, L. K. Ono, Z. Liu, T. Kim, T. Bouloumis, S. Kazaoui, Y. Qi, *J. Mater. Chem. A* **2019**, *7*, 6920.

[254] M. T. Hoerantner, E. L. Wassweiler, H. Zhang, A. Panda, M. Nasilowski, A. Osherov, R. Swartwout, A. E. Driscoll, N. S. Moody, M. G. Bawendi, K. F. Jensen, V. Bulović, *ACS Appl. Mater. Interfaces* **2019**, *11*, 32928.

[255] S. Razza, F. Di Giacomo, F. Matteocci, L. Cinà, A. L. Palma, S. Casaluci, P. Cameron, A. D'Epifanio, S. Licoccia, A. Reale, T. M. Brown, A. Di Carlo, *J. Power Sources* **2015**, *277*, 286.

[256] J. Li, H. Wang, X. Y. Chin, H. A. Dewi, K. Vergeer, T. W. Goh, J. W. M. Lim, J. H. Lew, K. P. Loh, C. Soci, T. C. Sum, H. J. Bolink, N. Mathews, S. Mhaisalkar, A. Bruno, *Joule* **2020**, *4*, 1035.

[257] X. Hou, Y. Wang, H. K. H. Lee, R. Datt, N. Uslar Miano, D. Yan, M. Li, F. Zhu, B. Hou, W. C. Tsoi, Z. Li, *J. Mater. Chem. A* **2020**, *8*, 21503.

[258] H. K. H. Lee, J. Barbé, S. M. P. Meroni, T. Du, C.-T. Lin, A. Pockett, J. Troughton, S. M. Jain, F. De Rossi, J. Baker, M. J. Carnie, M. A. McLachlan, T. M. Watson, J. R. Durrant, W. C. Tsoi, *Sol. RRL* **2019**, *3*, 1800207.

[259] X. Tian, S. D. Stranks, F. You, *Sci. Adv.* **2020**, *6*, eabb0055.

[260] European Commission, The RoHS Directive, https://ec.europa.eu/environment/topics/waste-and-recycling/rohs-directive_en (accessed: February 2021).

[261] N. Moody, S. Sesena, D. W. DeQuilettes, B. D. Dou, R. Swartwout, J. T. Buchman, A. Johnson, U. Eze, R. Brenes, M. Johnston, C. L. Haynes, V. Bulović, M. G. Bawendi, *Joule* **2020**, *4*, 970.

[262] Managing Hazardous Waste, https://dtsc.ca.gov/defining-hazardous-waste/ (accessed: February 2021).

[263] J. Li, H.-L. Cao, W.-B. Jiao, Q. Wang, M. Wei, I. Cantone, J. Lü, A. Abate, *Nat. Commun.* **2020**, *11*, 310.

[264] X. Li, F. Zhang, H. He, J. J. Berry, K. Zhu, T. Xu, *Nature* **2020**, *578*, 555.

[265] S. Y. Park, J. S. Park, B. J. Kim, H. Lee, A. Walsh, K. Zhu, D. H. Kim, H. S. Jung, *Nat. Sustain.* **2020**, *3*, 1044.

[266] R. L. Z. Hoye, L. C. Lee, R. C. Kurchin, T. N. Huq, K. H. L. Zhang, M. Sponseller, L. Nienhaus, R. E. Brandt, J. Jean, J. A. Polizzotti, A. Kursumović, M. G. Bawendi, V. Bulović, V. Stevanović, T. Buonassisi, J. L. MacManus-Driscoll, *Adv. Mater.* **2017**, *29*, 1702176.

[267] A. Babayigit, D. Duy Thanh, A. Ethirajan, J. Manca, M. Muller, H.-G. Boyen, B. Conings, *Sci. Rep.* **2016**, *6*, 18721.

[268] W.-F. Yang, J.-J. Cao, C. Dong, M. Li, Q.-S. Tian, Z.-K. Wang, L.-S. Liao, *Appl. Phys. Lett.* **2021**, *118*, 023501.

[269] N. Pai, J. Lu, T. R. Gengenbach, A. Seeber, A. S. R. Chesman, L. Jiang, D. C. Senevirathna, P. C. Andrews, U. Bach, Y. B. Cheng, A. N. Simonov, *Adv. Energy Mater.* **2019**, *9*, 1803396.

[270] J. Fisher, S. Benner, P. Golden, R. Edwards, Silver Toxicity: A Brief Overview, **2015**.

[271] J. Euvrard, X. Wang, T. Li, Y. Yan, D. B. Mitzi, *J. Mater. Chem. A* **2020**, *8*, 4049.

[272] M. Chen, M. G. Ju, A. D. Carl, Y. Zong, R. L. Grimm, J. Gu, X. C. Zeng, Y. Zhou, N. P. Padture, *Joule* **2018**, *2*, 558.

[273] I. Turkevych, S. Kazaoui, N. Shirakawa, N. Fukuda, *Jpn. J. Appl. Phys.* **2021**, *60*, SCCE06.

[274] A. Zakutayev, C. M. Caskey, A. N. Fioretti, D. S. Ginley, J. Vidal, V. Stevanovic, E. Tea, S. Lany, *J. Phys. Chem. Lett.* **2014**, *5*, 1117.

[275] R. E. Brandt, V. Stevanović, D. S. Ginley, T. Buonassisi, *MRS Commun.* **2015**, *5*, 265.

[276] R. C. Kurchin, P. Gorai, T. Buonassisi, V. Stevanović, *Chem. Mater.* **2018**, *30*, 5583.

[277] R. E. Brandt, J. R. Poindexter, P. Gorai, R. C. Kurchin, R. L. Z. Hoye, L. Nienhaus, M. W. B. Wilson, J. A. Polizzotti, R. Sereika, R. Žaltauskas, L. C. Lee, J. L. MacManus-Driscoll, M. Bawendi, V. Stevanović, T. Buonassisi, *Chem. Mater.* **2017**, *29*, 4667.

[278] A. Walsh, A. Zunger, *Nat. Mater.* **2017**, *16*, 964.

[279] Y.-T. Huang, S. R. Kavanagh, D. O. Scanlon, A. Walsh, R. L. Z. Hoye, *Nanotechnology* **2021**, *32*, 132004.

[280] L. C. Lee, T. N. Huq, J. L. MacManus-Driscoll, R. L. Z. Hoye, *APL Mater.* **2018**, *6*, 084502.

[281] V. Pecunia, L. G. Occhipinti, A. Chakraborty, Y. Pan, Y. Peng, *APL Mater.* **2020**, *8*, 100901.

[282] D. N. Dirin, L. Protesescu, D. Trummer, I. V. Kochetygov, S. Yakunin, F. Krumeich, N. P. Stadie, M. V. Kovalenko, *Nano Lett.* **2016**, *16*, 5866.

[283] A. M. Ganose, C. N. Savory, D. O. Scanlon, *Chem. Commun.* **2017**, *53*, 20.

[284] I. Turkevych, S. Kazaoui, E. Ito, T. Urano, K. Yamada, H. Tomiyasu, H. Yamagishi, M. Kondo, S. Aramaki, *ChemSusChem* **2017**, *10*, 3754.

[285] EU-Directive 2011/65/EU, *Off. J. Eur. Union* **2011**, *L174*, 88.

[286] R. Mohan, *Nat. Chem.* **2010**, *2*, 336.

[287] B. Saparov, F. Hong, J. P. Sun, H. S. Duan, W. Meng, S. Cameron, I. G. Hill, Y. Yan, D. B. Mitzi, *Chem. Mater.* **2015**, *27*, 5622.

[288] B. W. Park, B. Philippe, X. Zhang, H. Rensmo, G. Boschloo, E. M. J. Johansson, *Adv. Mater.* **2015**, *27*, 6806.

[289] M. Lyu, J. H. Yun, M. Cai, Y. Jiao, P. V. Bernhardt, M. Zhang, Q. Wang, A. Du, H. Wang, G. Liu, L. Wang, *Nano Res.* **2016**, *9*, 692.

[290] R. L. Z. Hoye, R. E. Brandt, A. Osherov, V. Stevanovic, S. D. Stranks, M. W. B. Wilson, H. Kim, A. J. Akey, J. D. Perkins, R. C. Kurchin, J. R. Poindexter, E. N. Wang, M. G. Bawendi, V. Bulovic, T. Buonassisi, *Chem. - Eur. J.* **2016**, *22*, 2605.

[291] S. Rieger, B. J. Bohn, M. Döblinger, A. F. Richter, Y. Tong, K. Wang, P. Müller-Buschbaum, L. Polavarapu, L. Leppert, J. K. Stolarczyk, J. Feldmann, *Phys. Rev. B* **2019**, *100*, 201404(R).

[292] J. P. Correa-Baena, L. Nienhaus, R. C. Kurchin, S. S. Shin, S. Wieghold, N. T. P. Hartono, M. Layurova, N. D. Klein, J. R. Poindexter, A. Polizzotti, S. Sun, M. G. Bawendi, T. Buonassisi, *Chem. Mater.* **2018**, *30*, 3734.

[293] R. L. Z. Hoye, J. Hidalgo, R. A. Jagt, J.-P. Correa-Baena, T. Fix, J. L. MacManus-Driscoll, *Adv. Energy Mater.* **2021**, 2100499, https://doi.org/10.1002/aenm.202100499.

[294] K. M. McCall, C. C. Stoumpos, O. Y. Kontsevoi, G. C. B. Alexander, B. W. Wessels, M. G. Kanatzidis, *Chem. Mater.* **2019**, *31*, 2644.

[295] K. M. McCall, C. C. Stoumpos, S. S. Kostina, M. G. Kanatzidis, B. W. Wessels, *Chem. Mater.* **2017**, *29*, 4129.

[296] F. Jiang, D. Yang, Y. Jiang, T. Liu, X. Zhao, Y. Ming, B. Luo, F. Qin, J. Fan, H. Han, L. Zhang, Y. Zhou, *J. Am. Chem. Soc.* **2018**, *140*, 1019.

[297] Y. Peng, F. Li, Y. Wang, Y. Li, R. L. Z. Hoye, L. Feng, K. Xia, V. Pecunia, *Appl. Mater. Today* **2020**, *19*, 100637.

[298] R. A. Jagt, T. N. Huq, K. M. Börsig, D. Sauven, L. C. Lee, J. L. MacManus-driscoll, R. L. Z. Hoye, *J. Mater. Chem. C* **2020**, *8*, 10791.

[299] E. T. Hoke, D. J. Slotcavage, E. R. Dohner, A. R. Bowring, H. I. Karunadasa, M. D. McGehee, *Chem. Sci.* **2015**, *6*, 613.

[300] L. Yu, A. Zunger, *Phys. Rev. Lett.* **2012**, *108*, 068701.

[301] T. N. Huq, L. C. Lee, L. Eyre, W. Li, R. A. Jagt, C. Kim, S. Fearn, V. Pecunia, F. Deschler, J. L. MacManus-Driscoll, R. L. Z. Hoye, *Adv. Funct. Mater.* **2020**, *30*, 1909983.

[302] S. S. Shin, J. P. Correa Baena, R. C. Kurchin, A. Polizzotti, J. J. Yoo, S. Wieghold, M. G. Bawendi, T. Buonassisi, *Chem. Mater.* **2018**, *30*, 336.

[303] W. Ke, M. G. Kanatzidis, *Nat. Commun.* **2019**, *10*, 965.

[304] W. Ke, C. C. Stoumpos, M. G. Kanatzidis, *Adv. Mater.* **2019**, *31*, 1803230.

[305] A. Goyal, S. McKechnie, D. Pashov, W. Tumas, M. Van Schilfgaarde, V. Stevanović, *Chem. Mater.* **2018**, *30*, 3920.

[306] F. Hao, C. C. Stoumpos, D. H. Cao, R. P. H. Chang, M. G. Kanatzidis, *Nat. Photonics* **2014**, *8*, 489.

[307] X. Jiang, F. Wang, Q. Wei, H. Li, Y. Shang, W. Zhou, C. Wang, P. Cheng, Q. Chen, L. Chen, Z. Ning, *Nat. Commun.* **2020**, *11*, 1245.

[308] H. Yao, F. Zhou, Z. Li, Z. Ci, L. Ding, Z. Jin, *Adv. Sci.* **2020**, *7*, 1903540.

[309] A. Abate, *Joule* **2017**, *1*, 659.

[310] A. Crovetto, A. Hajijafarassar, O. Hansen, B. Seger, I. Chorkendorff, P. C. K. Vesborg, *Chem. Mater.* **2020**, *32*, 3385.

[311] M. Khazaee, K. Sardashti, C. C. Chung, J. P. Sun, H. Zhou, E. Bergmann, W. A. Dunlap-Shohl, Q. Han, I. G. Hill, J. L. Jones, D. C. Lupascu, D. B. Mitzi, *J. Mater. Chem. A* **2019**, *7*, 2095.

[312] W. Rüdorff, H. Becker, *Z. Naturforsch., B: J. Chem. Sci.* **1954**, *9*, 614.

[313] A. R. Chakhmouradian, P. M. Woodward, *Phys. Chem. Miner.* **2014**, *41*, 387.

[314] H. C. Sansom, G. F. S. Whitehead, M. S. Dyer, M. Zanella, T. D. Manning, M. J. Pitcher, T. J. Whittles, V. R. Dhanak, J. Alaria, J. B. Claridge, M. J. Rosseinsky, *Chem. Mater.* **2017**, *29*, 1538.

[315] H. Zhu, M. Pan, M. B. Johansson, E. M. J. Johansson, *ChemSusChem* **2017**, *10*, 2592.

[316] Y. Kim, Z. Yang, A. Jain, O. Voznyy, G. H. Kim, M. Liu, L. N. Quan, F. P. García de Arquer, R. Comin, J. Z. Fan, E. H. Sargent, *Angew. Chem., Int. Ed.* **2016**, *55*, 9586; *Angew. Chem.* **2016**, *128*, 9738.

[317] J. Fisher, S. Benner, P. Golden, R. Edwards, Silver Toxicity: A Brief Overview, Boise, Idaho **2015**.

[318] T. Oldag, T. Aussieker, H. L. Keller, C. Preitschaft, A. Pfitzner, *Z. Anorg. Allg. Chem.* **2005**, *631*, 677.

[319] A. Pisoni, O. S. Baris, M. Spina, R. Gaa, *J. Phys. Chem. Lett.* **2014**, *5*, 2488.

[320] V. Pecunia, Y. Yuan, J. Zhao, K. Xia, Y. Wang, S. Duhm, L. Portilla, F. Li, *Nano-Micro Lett.* **2020**, *12*, 27.

[321] F. Wei, Z. Deng, S. Sun, F. Zhang, D. M. Evans, G. Kieslich, S. Tominaka, M. A. Carpenter, J. Zhang, P. D. Bristowe, A. K. Cheetham, *Chem. Mater.* **2017**, *29*, 1089.

[322] A. H. Slavney, T. Hu, A. M. Lindenberg, H. I. Karunadasa, *J. Am. Chem. Soc.* **2016**, *138*, 2138.

[323] R. L. Z. Hoye, L. Eyre, F. Wei, F. Brivio, A. Sadhanala, S. Sun, W. Li, K. H. L. Zhang, J. L. MacManus-Driscoll, P. D. Bristowe, R. H. Friend, A. K. Cheetham, F. Deschler, *Adv. Mater. Interfaces* **2018**, *5*, 1800464.

[324] Z. Li, S. Kavanagh, M. Napari, R. G. Palgrave, M. Abdi-Jalebi, Z. Andaji-Garmaroudi, D. W. Davies, M. Laitinen, J. Julin, M. A. Isaacs, R. H. Friend, D. O. Scanlon, A. Walsh, R. L. Z. Hoye, *J. Mater. Chem. A* **2020**, *8*, 21780.

[325] A. E. Maughan, A. M. Ganose, D. O. Scanlon, J. R. Neilson, *Chem. Mater.* **2019**, *31*, 1184.

[326] M. G. Ju, M. Chen, Y. Zhou, H. F. Garces, J. Dai, L. Ma, N. P. Padture, X. C. Zeng, *ACS Energy Lett.* **2018**, *3*, 297.

[327] D. Kong, D. Cheng, X. Wang, K. Zhang, H. Wang, K. Liu, H. Li, X. Sheng, L. Yin, *J. Mater. Chem. C* **2020**, *8*, 1591.

[328] D. Tiwari, D. Alibhai, D. J. Fermin, *ACS Energy Lett.* **2018**, *3*, 1882.

[329] W. A. Dunlap-Shohl, I. G. Hill, Y. Yan, D. B. Mitzi, *Chem. Mater.* **2018**, *30*, 8226.

[330] S. Weber, T. Rath, K. Fellner, R. Fischer, R. Resel, B. Kunert, T. Dimopoulos, A. Steinegger, G. Trimmel, *ACS Appl. Energy Mater.* **2019**, *2*, 539.

[331] F. Li, Y. Wang, K. Xia, R. L. Z. Hoye, V. Pecunia, *J. Mater. Chem. A* **2020**, *8*, 4396.

[332] Y. C. Choi, D. U. Lee, J. H. Noh, E. K. Kim, S. Il Seok, *Adv. Funct. Mater.* **2014**, *24*, 3587.

[333] R. Kondrotas, C. Chen, J. Tang, *Joule* **2018**, *2*, 857.

[334] Z. Yang, X. Wang, Y. Chen, Z. Zheng, Z. Chen, W. Xu, W. Liu, Y. (Michael) Yang, J. Zhao, T. Chen, H. Zhu, *Nat. Commun.* **2019**, *10*, 4540.

[335] H. Deng, Y. Zeng, M. Ishaq, S. Yuan, H. Zhang, X. Yang, M. Hou, U. Farooq, J. Huang, K. Sun, R. Webster, H. Wu, Z. Chen, F. Yi, H. Song, X. Hao, J. Tang, *Adv. Funct. Mater.* **2019**, *29*, 1901720.

Vincenzo Pecunia is an associate professor at the Institute of Functional Nano & Soft Materials, Soochow University, China. While being there, he founded and leads the Pecunia Group for Thin-Film Optoelectronics. Previously, he earned his Ph.D. in Physics and worked as a postdoctoral research associate at the Cavendish Laboratory, University of Cambridge, UK. His research interests include the charge transport physics and photoelectronic properties of environmentally friendly, solution-processed semiconductors, related optoelectronic devices (e.g., solar cells, photodetectors, and thin-film transistors), and their applications in printed optoelectronics.

Luigi G. Occhipinti is a director of research in graphene and related technologies and principal investigator at the Department of Engineering of the University of Cambridge, UK. He also serves as deputy director and chief operating officer of the Cambridge Graphene Centre, UK. He has developed science and innovation for 20+ yr in emerging technology areas for the post-CMOS roadmap, smart systems heterogeneous integration, polymer and printed electronics, advanced bio-systems and molecular diagnostics, advanced signal processing and nonlinear computation, advanced mechanical, and optical and chemical sensor technologies, with focus on miniaturization and advanced packaging technologies for smart devices and products.

Robert L. Z. Hoye is a lecturer (assistant professor) in Materials at Imperial College London. He also holds the Royal Academy of Engineering Research Fellowship. He completed his Ph.D. at the University of Cambridge (2012–2014), before working as a postdoctoral researcher at the Massachusetts Institute of Technology (2015–2016). He subsequently took up two Research Fellowships at Cambridge, firstly at Magdalene College (2016–2019), followed by Downing College (2019–2020), before taking up a lectureship at Imperial in 2020. His research focusses on defect-tolerant semiconductors, and their development into optoelectronic devices.